

# A Robust Bayesian Method for Polygenic Risk Scores using Projected Summary Statistics and Bridge Prior

Yuzheng Dun<sup>1</sup>, Nilanjan Chatterjee<sup>1,3</sup>, Jin Jin<sup>2,\*</sup>, and Akihiko Nishimura<sup>1,\*</sup>

<sup>1</sup>Department of Biostatistics, Bloomberg School of Public Health, Johns  
Hopkins University

<sup>2</sup>Department of Biostatistics, Epidemiology and Informatics, University of  
Pennsylvania

<sup>3</sup>Department of Oncology, School of Medicine, Johns Hopkins University

\*Corresponding authors: Akihiko Nishimura, [anishim2@jhu.edu](mailto:anishim2@jhu.edu); Jin Jin,  
[jin.jin@penmedicine.upenn.edu](mailto:jin.jin@penmedicine.upenn.edu)

## Abstract

Polygenic risk scores (PRS) developed from genome-wide association studies (GWAS) are of increasing interest for clinical and research applications. Bayesian methods have been popular for building PRS because of their natural ability to regularize models and incorporate external information. In this article, we present new theoretical results, methods, and extensive numerical studies to advance Bayesian methods for PRS applications. We identify a potential risk, under a common Bayesian PRS framework, of posterior impropriety when integrating the required GWAS summary-statistics and linkage disequilibrium (LD) data from two distinct sources. As a principled remedy to this problem, we propose a projection of the summary statistics data that ensures compatibility between the two sources and in turn a proper behavior of the posterior. We further introduce a new PRS method, with accompanying software package, under the less-explored Bayesian bridge prior to more flexibly model varying sparsity levels in effect size distributions. We extensively benchmark it against alternative Bayesian methods using both synthetic and real datasets, quantifying the impact of both prior specification and LD estimation strategy. Our proposed PRS-Bridge, equipped with the projection technique and flexible prior, demonstrates the most consistent and generally superior performance across a variety of scenarios.

*Keywords:* Continuous-shrinkage prior, genetic risk prediction, high-dimensional models, model regularization, prior pre-conditioning.

# 1 Introduction

Genome-wide association studies (GWAS) have identified tens of thousands of inherited variants explaining a considerable amount of variations in human traits and diseases across individuals [Seibert et al., 2018, Uffelmann et al., 2021]. Polygenic risk scores (PRS), constructed as weighted sums of the number of risk alleles for human traits and diseases, are of increasing interest in various research applications and clinical risk predictions [Chatterjee et al., 2016, Natarajan et al., 2017, Seibert et al., 2018, Khera et al., 2018, Torkamani et al., 2018, Lambert et al., 2019, Kullo et al., 2022]. At a basic level, the task of building PRS can be viewed as a high-dimensional regression problem for predicting outcome variables from hundreds of thousands or millions of genetic variants. Bayesian methods [de los Campos et al., 2010, Vilhjálmsón et al., 2015, Zhu and Stephens, 2017, Lloyd-Jones et al., 2019, Ge et al., 2019, Privé et al., 2020] have been popular in the PRS field as placing a prior on SNP effect sizes provides a natural way to introduce regularization and borrow external information [Hu et al., 2017, Márquez-Luna et al., 2021].

Despite its shared mathematical structure with standard regression problems, PRS development involves unique structures and challenges that complicate an application of existing Bayesian high-dimensional regression machinery. One challenge is the difficulty of access to sizable individual-level data. Correspondingly, PRS development typically relies on more accessible GWAS summary statistics data obtained from one-SNP-at-time regression. Reconstructing a multivariate regression model from the summary statistics then requires an estimate, typically obtained from external reference data, of linkage disequilibrium (LD) to account for correlations among genetic variants [Vilhjálmsón et al., 2015, Mak et al., 2017, Wang et al., 2020, Pattee and Pan, 2020, Chen et al., 2021]. This discrepancy in the data sources for GWAS summary statistics and LD estimate, if not properly

accounted for, leads to unexpected and potentially catastrophic inference as we establish in this article.

Another unique feature of PRS modeling is its unusual effect size distribution, or sparsity structure in regression coefficients. The high-dimensional regression literature typically assumes a relatively small number of the predictors explain most of the variation in the outcome. This is often not the case in polygenic prediction, however, where thousands to tens of thousands of small-effect genetic variants cumulatively contribute to prediction. Further, complex traits demonstrate a wide variety of genetic architectures [Zhang et al., 2018], calling for a prior with flexibility to adapt to a wide range of potential effect size distributions. While a range of prior families have been explored in the PRS literature [de los Campos et al., 2010, Vilhjálmsón et al., 2015, Zhu and Stephens, 2017, Ge et al., 2019, Privé et al., 2020], the impact of prior choice on model performance remains poorly understood since different methods have been benchmarked under different data sets and LD estimation strategies.

In this article, we make several important contributions to the Bayesian PRS literature. First, we identify and quantify a serious pitfall in the use of the commonly used approximate likelihood based on GWAS summary statistics and genetic correlation matrix from two distinct data sources. We show how the ill-defined nature of the approximate likelihood makes the inference susceptible to the prior choice or even produces an improper posterior. We then develop a principled solution to this ill-behavior, which in the past has been dealt with in an ad hoc manner such as by constraining the prior variance of regression coefficients [Ge et al., 2019]. Second, we introduce PRS-Bridge, a new PRS method based on the Bayesian Bridge prior [Polson et al., 2014] for flexible modeling of different genetic architectures. Compared to other commonly used shrinkage priors such as the popular horseshoe

prior [Carvalho et al., 2009], the Bridge prior better adapts to varying levels of sparsity and tail properties of effect size distribution through its exponent parameter. The Bridge prior also offers a major computational advantage as it allows for collapsed Gibbs sampling in posterior inference [Polson et al., 2014, Nishimura and Suchard, 2022]. Finally, we provide reliable evidence on the relative performance of different Bayesian PRS methods by carrying out one of the most systematic and comprehensive benchmark studies to date. We use both simulated and real datasets to compare PRS-Bridge against the two most popular Bayesian PRS methods, LDpred2 and PRS-CS, across a range of genetic architectures, data sources, and LD estimation strategies. Our benchmark study demonstrates PRS-Bridge’s compelling performance and a significant impact of LD estimation strategy on PRS methods’ performances. An optimized, open-source implementation of the algorithm is available on GitHub at <https://github.com/YuzhengDun1999/PRSBridge>.

## **2 Bayesian Regression Based on GWAS Summary Statistics and External LD Reference Data**

In this section, we lay out the general statistical model underlying the development of PRS based on GWAS summary data and external LD reference data. We will explain and quantify the statistical and computational ill-behavior that arise from the use of two separate data sources for summary statistics and LD reference data.

## 2.1 Likelihood Based on GWAS Summary Statistics and External LD Reference Data

When individual-level data is available, PRS model development can be viewed as a linear regression problem with the familiar mathematical structure:

$$\mathbf{y} = \mathbf{X}\boldsymbol{\beta} + \boldsymbol{\epsilon}, \quad \boldsymbol{\epsilon} \sim \mathcal{N}(\mathbf{0}, \sigma_{\epsilon}^2 \mathbf{I}), \quad (1)$$

where  $\mathbf{y}$  is the phenotype vector of  $N$  training individuals,  $\mathbf{X}$  the  $N \times P$  genotype matrix,  $\boldsymbol{\beta}$  the  $P$ -dimensional vector representing effect sizes of underlying genetic variants, and  $\boldsymbol{\epsilon}$  the error term. Typically, a set of genetic variants included in the PRS model comprises single nucleotide polymorphisms (SNPs), the most common type of DNA variations across individuals. The genotype of a SNP takes values of 0, 1, or 2 depending on the number of the risk allele copies carried by individuals in their two parental chromosomes. For the rest of our discussion in this section, we assume that both  $\mathbf{y}$  and  $\mathbf{X}$  have been centered and standardized.

While conceptually equivalent to a linear regression problem, PRS development is distinguished by its routine reliance on GWAS summary-level data instead of less accessible individual-level data. From standardized individual-level data, GWAS summary data is generated as estimates of marginal effect sizes through one-SNP-at-a-time regression:

$$\beta_{\text{sum},j} = \mathbf{x}_j^T \mathbf{y} / N \quad \text{for } j = 1, \dots, P,$$

where  $\mathbf{x}_j$  denotes the  $j$ -th column of the standardized genotype matrix  $\mathbf{X}$ . The model (1) for individual-level data implies that the likelihood of summary statistics is given by

$$\boldsymbol{\beta}_{\text{sum}} \mid \mathbf{X}, \sigma_{\epsilon}^2 \sim \mathcal{N}\left(\frac{\mathbf{X}^T \mathbf{X}}{N} \boldsymbol{\beta}, \frac{1 - h^2}{N} \frac{\mathbf{X}^T \mathbf{X}}{N}\right), \quad (2)$$

where  $h^2 = 1 - \sigma_{\epsilon}^2$  represents the amount of trait variation attributable to the additive effect of genetic variants and is referred to as heritability in population genetics.

We cannot, in practice, use the likelihood (2) to infer the effect size  $\beta$  since the summary statistics comes without the individual-level genotype matrix  $\mathbf{X}$  and thus without the empirical covariance  $\mathbf{X}^T \mathbf{X}$ . One way to get around this problem is to view the rows of  $\mathbf{X}$  as independent and identically distributed draws and take the expectation over this underlying population. Following the derivations in Zhu and Stephens [2017], we can then derive an approximate likelihood in terms of the population correlation  $\mathbf{D} = \mathbb{E}(\mathbf{X}^T \mathbf{X}/N)$ :

$$\beta_{\text{sum}} \mid \beta, \mathbf{D} \sim \mathcal{N}\left(\mathbf{D}\beta, \frac{\mathbf{D}}{N}\right), \quad (3)$$

where  $\mathbf{D}$  is typically referred to as the LD matrix in population genetics. We then substitute the population-level  $\mathbf{D}$  with an empirical estimate based on an external reference panel. For this purpose, we can use publicly available individual-level data, such as those through the popular 1000 Genomes (1000G) Project [Siva, 2008]. By substituting this estimated LD matrix  $\mathbf{D}_{\text{ref}} = \mathbf{X}_{\text{ref}}^T \mathbf{X}_{\text{ref}}/N_{\text{ref}}$  for  $\mathbf{D}$  in the likelihood (3), we obtain the following approximate likelihood based on GWAS summary data and external LD reference data:

$$\beta_{\text{sum}} \mid \beta, \mathbf{D}_{\text{ref}} \sim \mathcal{N}\left(\mathbf{D}_{\text{ref}}\beta, \frac{\mathbf{D}_{\text{ref}}}{N_{\text{train}}}\right). \quad (4)$$

Many of the existing PRS methods are based on the above approximate likelihood for summary statistics. As we will show in next section, however, this approximate likelihood is not a proper likelihood. Importantly, its naive use under the Bayesian framework results in a posterior distribution with unexpected and undesirable behavior.

## 2.2 Nominal Posterior’s Ill-behavior Caused by Mismatch between GWAS Summary Statistics and LD Reference Data Sources

In Section 2.1, we presented an approximate likelihood, widely used in the PRS problem, that combines summary data from one data source and LD matrix from another. We now show that the approximation can break down under a mismatch between the two data sources, leading to an unexpected and potentially catastrophic inference.

The issue stems from the fact that an empirical estimate  $\mathbf{D}_{\text{ref}}$  of a high-dimensional covariance matrix is unstable and, worse, often rank-deficient due to the limited reference sample size and high correlation among SNPs. When  $\mathbf{D}_{\text{ref}}$  is singular, the likelihood (4) represents a degenerate Gaussian distribution supported on the subspace  $\text{col}(\mathbf{D}_{\text{ref}}) \subsetneq \mathbb{R}^P$ , where  $\text{col}(\mathbf{D}_{\text{ref}})$  denotes the column space of  $\mathbf{D}_{\text{ref}}$ . This degeneracy is not a problem on its own; in fact, when  $\mathbf{D}_{\text{ref}}$  is estimated from the same data source as  $\boldsymbol{\beta}_{\text{sum}}$ , the likelihood makes sense because  $\boldsymbol{\beta}_{\text{sum}} = N_{\text{train}}^{-1} \mathbf{X}_{\text{ref}}^T \mathbf{y}_{\text{ref}}$  indeed lies in the column space of  $\mathbf{D}_{\text{ref}} = N_{\text{ref}}^{-1} \mathbf{X}_{\text{ref}}^T \mathbf{X}_{\text{ref}}$ . For  $\boldsymbol{\beta}_{\text{sum}}$  and  $\mathbf{D}_{\text{ref}}$  coming from two different data sources, however, it is likely to have a situation  $\boldsymbol{\beta}_{\text{sum}} \notin \text{col}(\mathbf{D}_{\text{ref}})$  — an impossible event under the specified likelihood. When this occurs, the approximate likelihood (4) makes no sense as a function of  $\boldsymbol{\beta}$ .

Curiously, if we were to ignore the ill-defined nature of the approximate likelihood, we can formally derive an apparently proper posterior distribution under a Gaussian prior  $\boldsymbol{\beta} \sim \mathcal{N}(\mathbf{0}, \boldsymbol{\Sigma}_0)$ . This posterior, which we call a *nominal* posterior, is given as follows:

$$\boldsymbol{\beta} \mid \boldsymbol{\beta}_{\text{sum}}, \mathbf{D}_{\text{ref}}, \boldsymbol{\Sigma}_0 \sim \mathcal{N}\left(\left(N_{\text{train}} \mathbf{D}_{\text{ref}} + \boldsymbol{\Sigma}_0^{-1}\right)^{-1} N_{\text{train}} \boldsymbol{\beta}_{\text{sum}}, \left(N_{\text{train}} \mathbf{D}_{\text{ref}} + \boldsymbol{\Sigma}_0^{-1}\right)^{-1}\right). \quad (5)$$

The apparent propriety of this nominal posterior likely explains why the ill-defined likelihood has so far been overlooked in the PRS literature. As we will show in Theorems 1 and



2 below, however, the nominal posterior exhibits highly problematic behaviors.

To state our theorem in a mathematically precise manner, we need one technical assumption. Denote  $\mathbf{D}_{\text{train}}$  as the sample correlation matrix obtained from the GWAS training samples. When the two column spaces  $\text{col}(\mathbf{D}_{\text{ref}}) = \text{col}(\mathbf{X}_{\text{ref}}^T)$  and  $\text{col}(\mathbf{D}_{\text{train}}) = \text{col}(\mathbf{X}_{\text{train}}^T)$  disagree, it is natural to expect  $\boldsymbol{\beta}_{\text{sum}} = N_{\text{train}}^{-1} \mathbf{X}_{\text{train}}^T \mathbf{y}_{\text{train}} \notin \text{col}(\mathbf{D}_{\text{ref}})$  but mathematically pathological cases hinder this conclusion. Assumption 1 below precludes such mathematical pathology and ensures in particular that, for any fixed non-zero vector  $\mathbf{v} \in \text{col}(\mathbf{D}_{\text{train}})$ , we have  $\langle \boldsymbol{\beta}_{\text{sum}}, \mathbf{v} \rangle \neq 0$  with probability one:

**Assumption 1.** The probability distribution  $\mathbf{y}_{\text{train}} \mid \mathbf{X}_{\text{train}}$  underlying the individual-level data is absolutely continuous with respect to the Lebesgue measure in  $\mathbb{R}^N$ .

With the technical assumption above, we are now ready to state our theorem:

**Theorem 1.** *The following result holds for almost every realization of  $\boldsymbol{\beta}_{\text{sum}}$  under Assumption 1. Consider the posterior distribution  $\boldsymbol{\beta} \mid \boldsymbol{\beta}_{\text{sum}}, \mathbf{D}_{\text{ref}}, \sigma_0$  based on the prior  $\boldsymbol{\beta} \mid \sigma_0 \sim \mathcal{N}(\mathbf{0}, \sigma_0^2 \mathbf{I})$  with standard deviation  $\sigma_0 > 0$ . If  $\text{null}(\mathbf{D}_{\text{ref}}) \not\subseteq \text{null}(\mathbf{D}_{\text{train}})$ , then the posterior mean  $\hat{\boldsymbol{\beta}}(\sigma_0) = \mathbb{E}[\boldsymbol{\beta} \mid \boldsymbol{\beta}_{\text{sum}}, \mathbf{D}_{\text{ref}}, \sigma_0]$  diverges in the limit of the prior becoming uninformative; i.e.,  $\|\hat{\boldsymbol{\beta}}(\sigma_0)\|^2 \rightarrow \infty$  as  $\sigma_0 \rightarrow \infty$ . No such pathological behavior occurs when  $\mathbf{D}_{\text{ref}} = \mathbf{D}_{\text{train}}$  or, more generally, when  $\text{null}(\mathbf{D}_{\text{ref}}) \subseteq \text{null}(\mathbf{D}_{\text{train}})$ .*

The proof is in Appendix Section A.

Ordinarily, when fitting a linear regression model of the form (1) under the prior  $\boldsymbol{\beta} \mid \sigma_0 \sim \mathcal{N}(\mathbf{0}, \sigma_0^2 \mathbf{I})$ , the posterior mean converges to a finite limit as  $\sigma_0 \rightarrow \infty$ ; this is true even when  $N < p$ . Theorem 1 shows that the nominal posterior (5) defies this expected behavior and pulls the posterior estimate towards infinity when there is a mismatch between the LD reference and GWAS training samples. The analysis in Appendix Section A reveals that this is caused by the approximate likelihood (4) being falsely informative in the null

space of  $\mathbf{D}_{\text{ref}} = \mathbf{X}_{\text{ref}}^T \mathbf{X}_{\text{ref}} / N_{\text{ref}}$ . Theorem 2 below shows that this undesirable feature of the approximate likelihood leads to an even more serious, and insidious, problem of potential posterior impropriety when placing a Gaussian scale-mixture prior on  $\boldsymbol{\beta}$ .

To deal with high-dimensionality of the problem, Bayesian PRS methods typically deploy a sparsity-inducing prior on  $\boldsymbol{\beta}$  with a scale-mixture representation  $\beta_j \mid \tau, \lambda_j \sim \mathcal{N}(0, \tau^2 \lambda_j^2)$  with global scale  $\tau$ , which we presently assume to be fixed to simplify the presentation, and local scale  $\lambda_j \sim \pi(\lambda_j)$ . The posterior inference based on these methods typically relies on a Gibbs sampler, alternately sampling from the nominal posterior of (5) with  $\boldsymbol{\Sigma}_0 = \tau^2 \boldsymbol{\Lambda}^2$  for  $\boldsymbol{\Lambda} = \text{diag}(\lambda_1, \dots, \lambda_P)$  and from  $\boldsymbol{\lambda} \mid \boldsymbol{\beta}, \tau$ . This Gibbs sampler may never converge, however; two proper conditional distributions do not necessarily form a proper joint distribution [Gelman and Speed, 1993, Hobert and Casella, 1998]. This is a particularly germane concern given the ill-defined nature of the approximate likelihood under the data mismatch.

The joint posterior distribution, if it exists, can be expressed in terms of the conditional distributions as

$$\pi(\boldsymbol{\beta}, \boldsymbol{\lambda} \mid \boldsymbol{\beta}_{\text{sum}}, \mathbf{D}_{\text{ref}}, \tau) \propto \frac{\pi(\boldsymbol{\beta} \mid \boldsymbol{\lambda}, \boldsymbol{\beta}_{\text{sum}}, \mathbf{D}_{\text{ref}}, \tau) \pi(\boldsymbol{\lambda} \mid \hat{\boldsymbol{\beta}}, \boldsymbol{\beta}_{\text{sum}}, \mathbf{D}_{\text{ref}}, \tau)}{\pi(\hat{\boldsymbol{\beta}} \mid \boldsymbol{\Sigma}_0, \boldsymbol{\beta}_{\text{sum}}, \mathbf{D}_{\text{ref}}, \tau)} \quad (6)$$

for any  $\hat{\boldsymbol{\beta}}$  [Gelman and Speed, 1993]. We will refer to the potentially improper density function satisfying the above relation as the *joint nominal posterior*. We show below that, if the prior on  $\beta_j$  has a tail that decays slower than exponential, then the joint nominal posterior is improper under the mismatched case. Importantly, while each of the two conditional distributions is well-defined on its own, the Gibbs sampler alternately sampling from each never converges.

**Theorem 2.** *The following result holds for almost every realization of  $\boldsymbol{\beta}_{\text{sum}}$  under Assumption 1. Consider a joint nominal posterior distribution  $\boldsymbol{\beta}, \lambda_1^2, \dots, \lambda_P^2 \mid \boldsymbol{\beta}_{\text{sum}}, \mathbf{D}_{\text{ref}}, \tau$*

under a heavy-tailed prior on  $\beta_j$  represented as a scale-mixture  $\beta_j | \tau, \lambda_j \sim \mathcal{N}(0, \tau^2 \lambda_j^2)$  with  $\lambda_j \sim \pi(\lambda_j)$ . If  $\text{null}(\mathbf{D}_{\text{ref}}) \not\subset \text{null}(\mathbf{D}_{\text{train}})$ , then the joint nominal posterior is improper. On the other hand, the joint nominal posterior is proper when  $\mathbf{D}_{\text{ref}} = \mathbf{D}_{\text{train}}$  or, more generally, when  $\text{null}(\mathbf{D}_{\text{ref}}) \subset \text{null}(\mathbf{D}_{\text{train}})$ .

The proof, along with a formal definition of heavy-tailed distributions, is in Appendix B.

### 2.3 Real Data Demonstrations of Danger from Data Mismatch

In Section 2.2, we have theoretically characterized the ill-behavior arising from the use of the approximate likelihood in the presence of a mismatch between LD reference and GWAS training samples. We now demonstrate, using a real dataset and existing Bayesian PRS software, that this issue has a real consequence in application.

We obtain GWAS summary statistics for BMI from approximately 290K unrelated European individuals in UK Biobank. We download, from the PRS-CS website, the LD matrix estimated from 503 European individuals in 1000G. We then run PRS-CS on this dataset; we use the software provided by Ge et al. [2019] as is except for the one-liner change, as described below, to remove the ad-hoc constraint on the prior variance of regression coefficients.

The Strawderman-Berger prior used in PRS-CS is heavy-tailed and, by Theorem 2, yields an improper posterior under the data mismatch. The resulting breakdown of posterior inference, though *not* its root cause, has likely been known to the authors of PRS-CS as Ge et al. [2019] propose to impose a constraint  $\tau^2 \lambda_j^2 \leq \sigma_{\text{bd}}^2$  on the prior variance of  $\beta_j$  for some fixed  $\sigma_{\text{bd}}$ . They explain this constraint as necessary to deal with co-linearity among SNPs, but this logic is faulty: while problematic in its own way, co-linearity will not cause an improper posterior under a proper prior. Figure 1 shows traceplots of the

regression coefficients when the constraint is removed. Since the Gibbs sampler is actually sampling from an improper target, the coefficients start exploding at some point with its values exceeding  $10^{20}$  in magnitudes. When run longer, the software breaks down before long due to numerical errors.

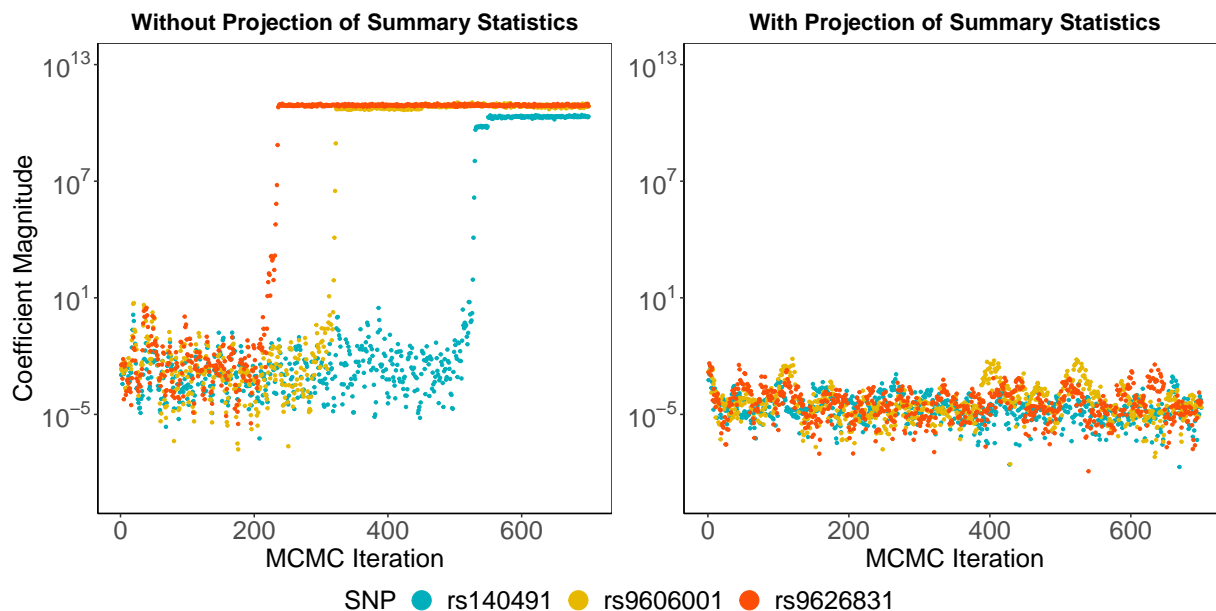


Figure 1: Traceplots of the samples, corresponding to the first three coefficients to explode, generated by PRS-CS when removing the ad-hoc constraint on the prior variance. The summary statistics is taken from UK Biobank and the LD matrix from 1000G. The data mismatch results in impropriety of the joint nominal posterior and in the explosion of the Gibbs sampler. The software breaks down after a while due to numerical errors. The use of projected summary statistics ensures proper posterior inference.

While the constraint  $\tau^2 \lambda_j^2 \leq \sigma_{\text{bd}}^2$  does ensure posterior propriety, this ad hoc solution only indirectly addresses the fundamental problem of the ill-defined approximate likelihood (4). One practical concern is the posterior inference’s sensitivity to the choice of the bound  $\sigma_{\text{bd}}$  since, as our theory tells us, this constraint is the only thing preventing the posterior from becoming improper. When using this thresholding approach, therefore,  $\sigma_{\text{bd}}$

should really be considered as a potential tuning parameter, rather than assuming  $\sigma_{\text{bd}} = 1$  proposed casually as default by Ge et al. [2019] to work well in all applications. We demonstrate the inference’s sensitivity to  $\sigma_{\text{bd}}$  in next section.

## 2.4 Projected GWAS Summary Statistics

Having demonstrated the posterior ill-behavior caused by data mismatch, we now turn to providing a statistically principled solution to the problem. The theoretical results of Section 2.2 characterize the ill-behavior as caused by the summary statistics lying outside the column space of the reference LD matrix. This insight motivates the following approach based on a linear projection of summary statistics. The idea is to treat the approximate likelihood (4) as a likelihood not for the raw summary statistics  $\boldsymbol{\beta}_{\text{sum}}$  but for its projection  $\mathbf{P}_{\text{ref}}\boldsymbol{\beta}_{\text{sum}}$  onto  $\text{col}(\mathbf{D}_{\text{ref}})$ . This projection can be expressed, in terms of the eigenvectors  $\mathbf{v}_1, \mathbf{v}_2, \dots, \mathbf{v}_K$  associated with the non-zero eigenvalues of  $\mathbf{D}_{\text{ref}}$ , as

$$\mathbf{P}_{\text{ref}}\boldsymbol{\beta}_{\text{sum}} = \sum_{k=1}^K \langle \boldsymbol{\beta}_{\text{sum}}, \mathbf{v}_k \rangle \mathbf{v}_k.$$

The projected summary statistics is guaranteed to lie in the support of the approximate likelihood (4) and its use in place of the raw one, therefore, ensures a proper inference.

This projection approach can be applied to any PRS methods to avoid the posterior ill-behavior. For illustration, we modify PRS-CS to use the projected summary statistics. This modified version yields a sound posterior inference without the constraint on the prior variance, as evidenced in the traceplots on the right panel of Figure 1, since the posterior is now guaranteed to be proper. We also compare its performance to the original PRS-CS based on the ad hoc constraint  $\tau^2\lambda_j^2 \leq \sigma_{\text{bd}}^2$ , where we vary  $\sigma_{\text{bd}} = 0.1, 1,$  and  $10$  to assess the inference’s sensitivity to  $\sigma_{\text{bd}}$ . The results from this comparison, presented in Supplementary Figure 2, confirm that the performance of the original PRS-CS is sensitive to the choice of

$\sigma_{\text{bd}}$ , while our projection approach leads to a more consistent and competitive performance.

## 3 Methods

### 3.1 Existing Bayesian PRS methods: LDpred2 and PRS-CS

We first review the two most popular Bayesian PRS methods: LDpred2 and PRS-CS.

LDpred (Vilhjalmsson et al. [2015]) models the effect size distribution of SNPs with a spike-and-slab prior in the form,

$$\beta_j \sim \begin{cases} \mathcal{N}\left(0, \frac{h^2}{\varpi P}\right) & \text{with probability } \varpi, \\ 0 & \text{otherwise,} \end{cases} \quad (7)$$

where  $P$  denotes the total number of SNPs,  $\varpi$  the causal SNP proportion, and  $h^2$  the total heritability. Its successor LDpred2 adopts the same model but provides a faster and more robust implementation [Prive et al., 2018]. LDpred2-grid estimates them based on the predictive performance of the corresponding PRS model on a tuning dataset, while LDpred2-auto estimates them in a fully Bayesian manner.

PRS-CS [Ge et al., 2019] is another popular Bayesian PRS method. It adopts a global-local shrinkage prior known as the Strawderman-Berger prior:

$$\beta_j | \tau, \lambda_j \sim \mathcal{N}\left(0, \frac{\sigma^2}{N} \tau^2 \lambda_j^2\right) \text{ for } \pi(\lambda_j) = \frac{\lambda_j}{(1 + \lambda_j^2)^{\frac{3}{2}}} \text{ on } \lambda_j \geq 0,$$

where global scale  $\tau$  controls the overall sparsity level and local scales  $\lambda_j$  allow variations in effect size magnitudes. The PRS-CS software provides an option to estimates  $\tau$  in a fully Bayesian manner with a half-Cauchy prior. The global scale is otherwise treated as a tuning parameter and estimated based on the prediction performance on a tuning dataset.

## 3.2 PRS-Bridge: Robust, Flexible, and Scalable PRS Method

We now introduce our PRS-Bridge, a new method with accompanying software that combines the summary statistics projection approach of Section 2.4 with the flexibility of the Bridge prior having a powered exponential distribution of the form

$$\beta_j | \tau \propto \tau^{-1} \exp\left(-\left|\frac{\beta_j}{\tau}\right|^\alpha\right) \text{ for } \alpha > 0.$$

Importantly, the exponent parameter  $\alpha$  gives the Bridge prior an ability to adapt to different degrees of sparsity in the effect sizes and hence to different genetic architectures. This flexibility is a major advantage over the other priors previously considered in the PRS literature. We treat  $\alpha$  as a tuning parameter and select an optimal value based on the performance on a tuning dataset. We find the candidate values of  $\alpha \in \{0.125, 0.25, 0.5\}$  to provide sufficient flexibility in the PRS application.

Figure 2 illustrates with contour plots the flexibility offered by the Bridge prior’s exponent parameter. When  $\alpha = 1$ , the prior coincides with the Laplace distribution and the model recovers the Bayesian lasso [Park and Casella, 2008]. As  $\alpha \rightarrow 0$ , the prior becomes more peaked at 0 and heavier-tailed at the same time, inducing an increasingly sparser structure in the SNP effect size distribution. On the other hand, the Strawderman-Berger prior used by PRS-CS has a fixed sparsity structure.

The Bridge prior also has a major computational advantage over other continuous shrinkage priors due to the availability of a collapsed update of the global scale parameter  $\tau$  within the Gibbs sampler (Polson et al. [2014]). Polson et al. [2014] show that this collapsed Gibbs sampler generates samples with little autocorrelation even when the posterior computation under other shrinkage priors suffers from poor mixing. This efficiency gain is particularly valuable given the high computational demands of the PRS application.

For further scalability, our implementation of the PRS-Bridge method deploys the con-

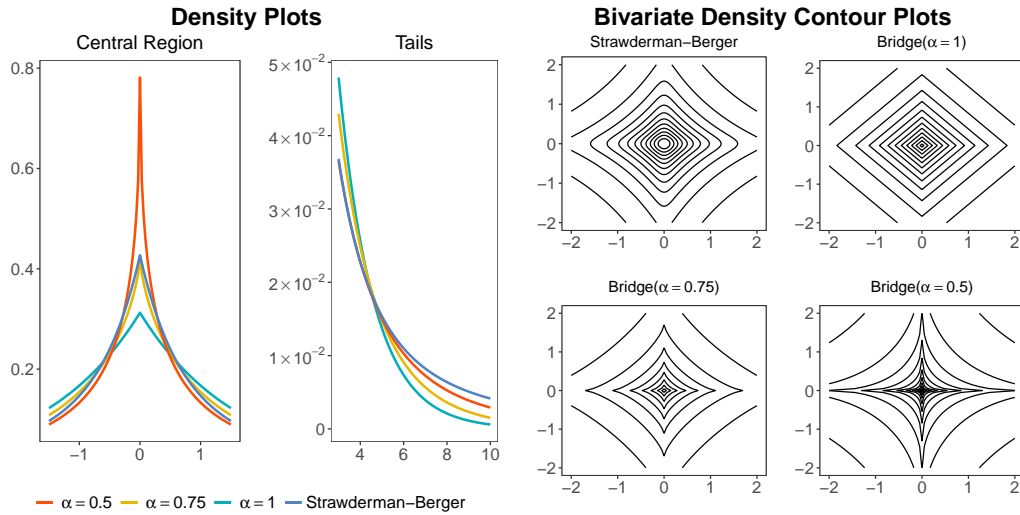


Figure 2: Comparison of the Strawderman-Berger prior used in PRS-CS and the Bridge prior under varying  $\alpha$  values. In the left plot, the different priors are scaled to have the same amount of probability in the region  $[-2, 2]$  to facilitate the comparison.

jugate gradient (CG) sampler of Nishimura and Suchard [2022] within the collapsed Gibbs sampler. The CG sampler speeds up the computation by transforming the task of sampling from a high-dimensional multivariate Gaussian into that of solving a deterministic linear system, to which the CG algorithm can be applied. For the PRS posterior, the main cost of the CG step is the iterative application of the matrix-vector operation  $\mathbf{v} \rightarrow \mathbf{D}\mathbf{v}$  by the LD matrix. This allows us to exploit the structured LD approximations discussed in Section 3.3. Further details on the posterior computation under PRS-Bridge is provided in Appendix D.

### 3.3 LD Approximation Strategy

Population genetic theory predicts that SNPs far apart in the genome are likely to be independent due to recombinations. An Empirical estimate of SNP-correlation matrix,



also referred to LD matrix, shows expected patterns of sparsity (Supplementary Figure 3). It is common for PRS methods, therefore, to impose a sparsity structure in approximating the population LD matrix and try taking advantage of it in the computation. Existing methods have explored various sparsity structures, such as banded and block diagonal approximations [Vilhjálmsson et al., 2015, Mak et al., 2017, Ge et al., 2019, Privé et al., 2020]. The block diagonal approximation, for example, allows each corresponding block of regression coefficients to be updated independently.

The projection of the summary statistics proposed in Section 2.4 offers an opportunity to additionally approximate the LD matrix through a low-rank structure, which can be combined with the block diagonal approximation. Specifically, we selectively keep  $K^* \leq K$  largest eigenvalues of LD matrix and disregard relatively smaller eigenvalues. The low-rank approximated LD matrix will be  $\mathbf{D}_{\text{ref}} = \sum_{k=1}^{K^*} \lambda_k \mathbf{v}_k \mathbf{v}_k^T$ , where  $\lambda_k$  is the eigenvalues of LD matrix corresponding to eigenvector  $\mathbf{v}_k$ . This low-rank approximation can speed up the posterior computation based on the CG sampler. In our implementation of PRS-Bridge, we treat the percentage of eigenvalues removed as a tuning parameter and find that low-rank approximation improves not only computational but also statistical efficiency.

The impacts of LD approximation strategies on PRS methods’ statistical performance have been understudied. In our numerical study, we investigate impacts of using different LD approximation strategies in each PRS methods. PRS-CS implements a block approximation of the LD matrix by partitioning the whole genome into nearly independent LD blocks of fixed sizes. For PRS-Bridge, we implement the same block approximation strategies but with additional flexibility to use larger LD block sizes. LDpred2 offers an option to use either the larger block approximation or banded approximation that only accounts for correlation within a neighboring LD region of each SNP. Details of the choice of LD

reference data and sparse LD structures are summarized in Appendix F.

## 4 Numerical Studies

### 4.1 Plasmode Synthetic Data from Spike-and-slab Model

We first compare performances of LDpred2, PRS-CS, and PRS-Bridge on the synthetic large-scale datasets of Zhang et al. [2023]; these are “plasmode” datasets [Gadbury et al., 2008], mimicking essential features of real data such LD structures and SNP proportions to allow for realistic evaluation. The genotype data of 120,000 individuals are simulated, using HAPGEN2 version 2.1.2 [Su et al., 2011], to mimic the 1000G reference data containing 498 unrelated individuals of European ancestry [Siva, 2008]. Trait values for the individuals are simulated from a linear model with SNP effect sizes generated from a spike-and-slab distribution. This effect size distribution coincides with the assumption of LDpred2, tilting the simulation study in its favor.

We design the synthetic datasets to cover a range of genetic architectures by varying proportions of non-null SNPs and effect sizes’ relationship to allele frequencies as results of negative selection. We use a random subset of 100,000 individuals to generate the GWAS summary statistics for training, 10,000 for parameter tuning, and 10,000 for calculating out-of-sample prediction performance. The LD matrix is estimated from the 1000G reference data. Details of the method implementation are summarized in Appendix E.

Figure 3 compares the out-of-sample prediction performance of the three PRS methods under the variety of genetic architectures. Unsurprisingly, since the datasets are simulated under the spike-and-slab model, correctly specified LDpred2 performs the best. On the other hand, PRS-Bridge’s performance is remarkably close despite its misspecification of the

effect size distribution. In particular, PRS-Bridge outperforms PRS-CS consistently and by substantial margins. The flexibility provided by the Bridge prior's exponent parameter  $\alpha$  appears to play a major role in its superior performance. In fact, as the true causal SNP proportions decrease, so does the optimal  $\alpha$  selected during the tuning process reflecting with the role of  $\alpha$  in controlling the prior sparsity level.

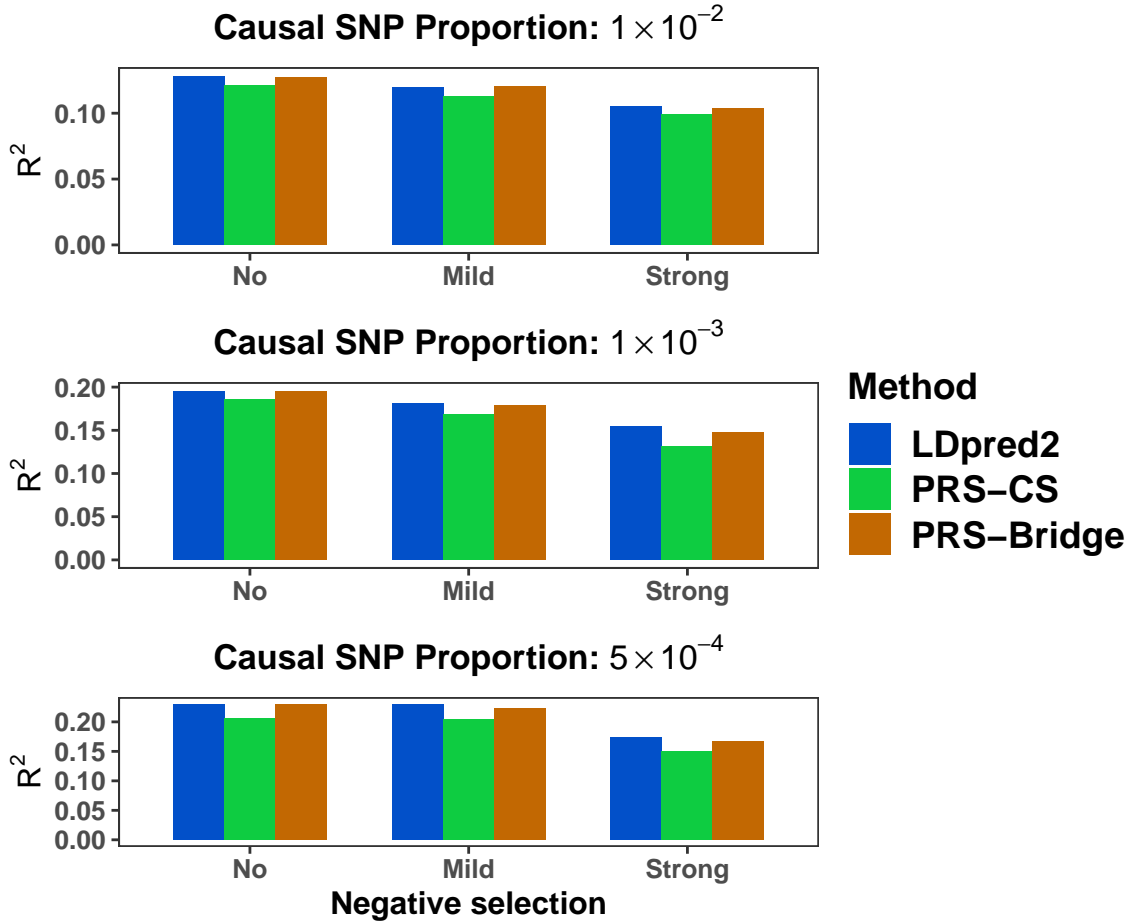


Figure 3: Comparison of out-of-sample prediction performances, reported in terms of  $R^2$ , by LDpred2, PRS-CS, and PRS-Bridge on the plasmode synthetic datasets. The causal SNP proportions are varied from 0.01, 0.001, to 0.0005. The effect sizes of causal variants are assumed to be related to allele frequency under a model with no, mild, or strong negative selection. The LDpred2 software uses a banded LD structure with the default LD radius of 3cM. The PRS-CS and PRS-Bridge implementations use the block-diagonal LD approximation, with PRS-Bridge additionally using low-rank approximation.

## 4.2 Real Data Benchmark on Continuous Traits from UK Biobank

We now apply the three PRS methods to data from UK Biobank to develop PRS for six continuous human traits: BMI, resting heart rate, high-density and low-density lipoprotein cholesterol, apolipoprotein A1, and apolipoprotein B. We take 319,342 unrelated European individuals from UK Biobank and use 90/5/5% of the data as: a training set of 287,285 individuals to obtain summary data; a tuning set of 16,028 individuals to select tuning parameters; and a validation set of 16,029 individuals to calculate out-of-sample prediction  $R^2$ . We adjust for age, gender, and the top 10 genetic principal components besides genotype. To assess how the choice of external reference data affects PRS methods' performance, we implement each method using two different data sources, UK Biobank or 1000G, for estimating the LD matrix.

Figure 4 summarizes the results of our benchmark study on continuous traits. PRS-Bridge shows the best overall performance when treating the LD block size as a tuning parameter. When using the relatively large LD reference data from UK Biobank, the large-block PRS-Bridge outperforms the default-setting PRS-CS with an average  $R^2$  increase of 14.83%, the banded LDpred2 by 2.29%, and the large-block LDpred2 by 3.20%. When using the smaller 1000G LD reference data, the small-block PRS-Bridge exhibits similar performance to the default-setting PRS-CS and outperforms the banded LDpred2 with an average  $R^2$  increase of 28.42%. We further compare the computational efficiency of these methods in Appendix H.

When using 1000G as a reference database, the prediction power of all methods decreases compared to using UK Biobank. This is unsurprising since 1000G provides far fewer samples than UK Biobank ( $N \approx 500$  vs.  $N \approx 330K$ ) to estimate the LD matrix. PRS-Bridge and PRS-CS nonetheless show performance more robust to the choice of LD

reference samples than LDpred2. Our results also show that the smaller LD reference sample size warrants more regularization in the LD matrix estimation using a smaller block size. When using UK Biobank as reference, the large-block PRS-Bridge on average yields 2.72% improvement in prediction over the smaller-block one. On the other hand, when using 1000G as reference, the small-block PRS-Bridge outperforms the larger-block one, with 28.64% improvement on average.

### 4.3 Real Data Benchmark on Binary Traits using Summary Statistics from External Sources

We now benchmark the three PRS methods on the following five disease traits: breast cancer, coronary artery disease, depression, rheumatoid arthritis, and inflammatory bowel disease. For binary disease outcomes, even the largest biobanks such as UK Biobank lack an adequate number of cases and sufficient statistical power. For this reason, we train the PRS models on publicly available GWAS summary data from external sources and evaluate their predictive performances on individual-level validation samples from UK Biobank; Supplementary Table 2 provides a detailed description of the summary data sources as well as the sample sizes of training, tuning, and validation sets. We evaluated AUC and compare model performance using the scale  $2\{\Phi^{-1}(AUC)\}^2$ , where  $\Phi$  is the standard Gaussian cumulative distribution function. This scale reflects the variation of the risk of the disease explained in the log-risk scale [Pharoah et al., 2002] and helps to quantify the “relative-efficiency” of methods in the sense of sample-size requirement for equivalent predictive power [Chatterjee et al., 2013].

Figure 5 summarizes the results of our benchmark study on binary disease traits. The results here show the same patterns as in our study on continuous traits: PRS-Bridge

generally outperforms LDpred2 and PRS-CS; the larger LD reference sample size leads to better performances; and PRS-Bridge and PRS-CS are more robust than LDpred2 to the choice of reference data. PRS-Bridge's predictive ability for coronary artery disease and inflammatory bowel disease are particularly remarkable. When using UK Biobank as reference, the larger-block PRS-Bridge delivers 18.5% improvement in predicting coronary artery disease over the best performing LDpred2 and 25.7% improvement over PRS-CS. In predicting inflammatory bowel disease, the improvement is 40.0% over the best performing LDpred2 and 34.5% over PRS-CS.

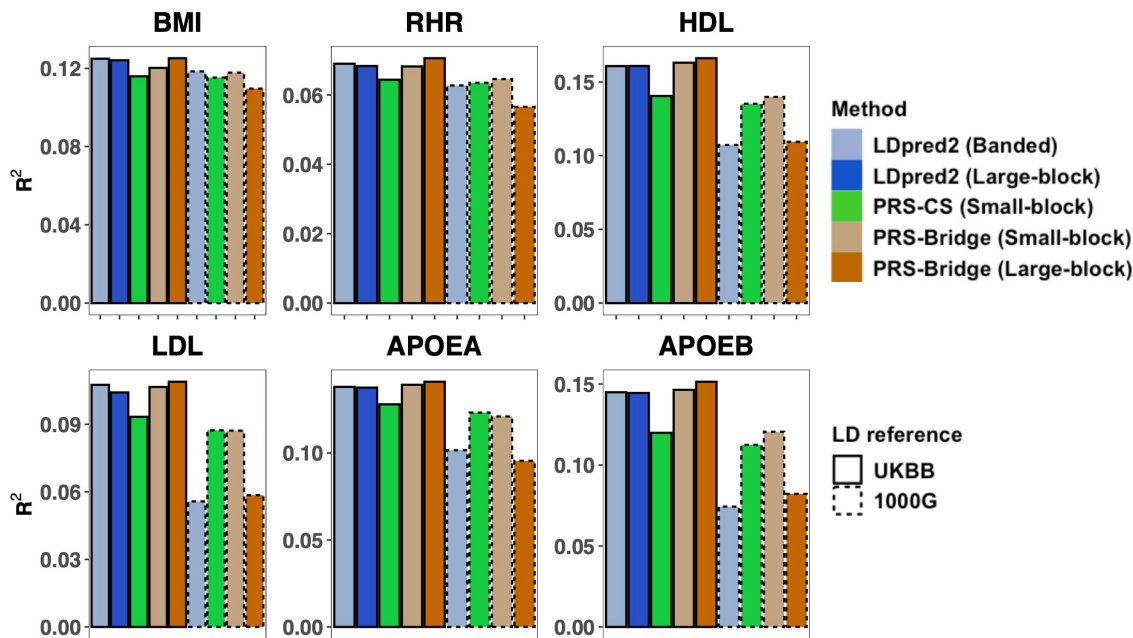


Figure 4: Out-of-sample prediction  $R^2$  of LDpred2, PRS-CS, and PRS-Bridge on the six continuous traits: BMI, resting heart rate (RHR), high-density lipoprotein cholesterol (HDL), low-density lipoprotein cholesterol (LDL), apolipoprotein A1 (APOEA), and apolipoprotein B (APOEB). We implement each method with two alternative LD reference data sources, 1000G and UK Biobank. “(Banded)” indicates the use of the banded structure in approximating LD, while “(Small-block)” and “(Large-block)” indicate the use of the block structure with the small and large blocks. For LDpred2 and PRS-CS, we only consider the default LD structures in their software.



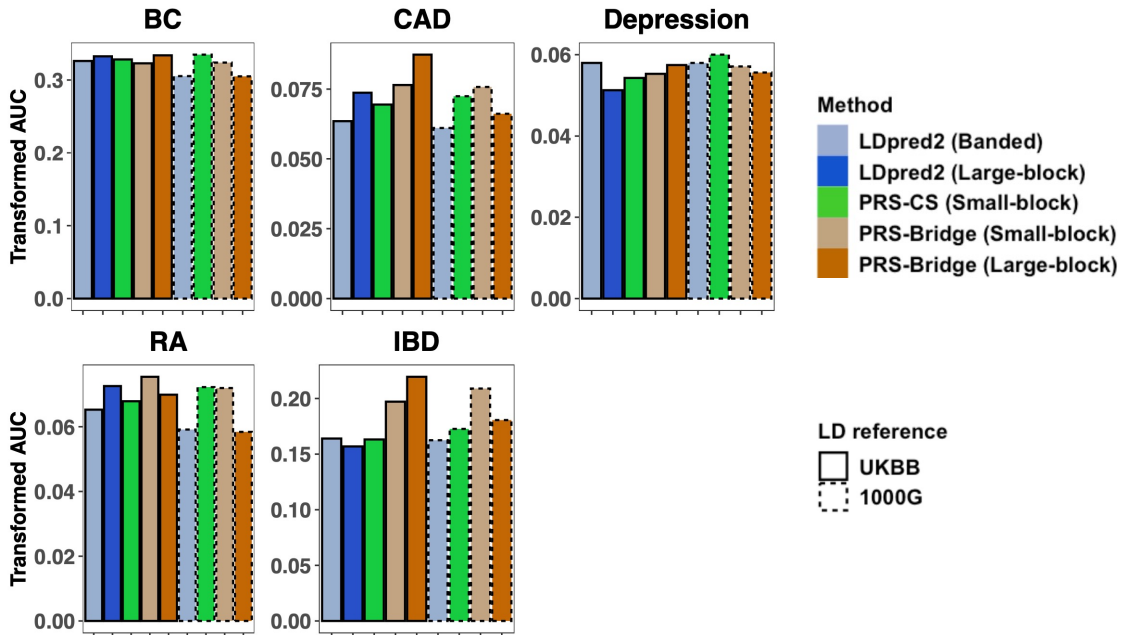


Figure 5: Out-of-sample prediction performances of LDpred2, PRS-CS, and PRS-Bridge on the five binary disease traits: breast cancer (BC), coronary artery disease (CAD), depression, rheumatoid arthritis (RA), and inflammatory bowel disease (IBD). The methods are implemented in the same manners as described in the Figure 4 caption.

## 5 Discussion

This work advances the Bayesian PRS methodology on multiple fronts. We have uncovered a previously overlooked pitfall in the widely used approach based on the approximate likelihood and proposed a principled remedy via the projection of GWAS summary statistics. While in the current study we focus on applications involving PRS development, the issue is also relevant for Bayesian methods for other applications like fine-mapping of causal variants within genomic regions [Wang et al., 2020, Yang et al., 2023]. We have further demonstrated, through an extensive numerical study, an opportunity to improve PRS performance by more carefully considering the choice of a prior on SNP effect size

distribution, of reference data for estimating LD, and of a structured approximation of LD. Our proposed PRS-Bridge delivers consistent and superior performance thanks to its use of the projected summary statistics and the Bridge prior’s flexibility to adapt to varying effect size distributions. In our real data analyses, PRS-Bridge demonstrates a meaningful increase in predictive power over LDPred2 and PRS-CS for a number of clinically relevant traits such as coronary artery disease and inflammatory bowel disease.

As PRS methodology moves in the direction of joint modeling across diverse ancestry groups and related traits, we expect the use of a flexible prior to become even more important in capturing a range of multivariate SNP effect size distributions. Another direction is the choice of prior that will allow flexible incorporation of functional annotation information on genetic variants derived from external data. Bayesian approaches to PRS have much potential, and further advances in the methodology can help realize the full potential of genomic medicine.

## Data and Code Availability

The plasmode synthetic data used in Section 4 are publicly available at <https://doi.org/10.7910/DVN/COXHAP>, the UK Biobank data at <https://www.ukbiobank.ac.uk/>, and the 1000G data at [https://mathgen.stats.ox.ac.uk/impute/1000GP\\_Phase3.html](https://mathgen.stats.ox.ac.uk/impute/1000GP_Phase3.html). All the GWAS summary statistics of the binary disease traits are also publicly available with details provided in Supplementary Table 2. A Python-based command line tool for the implementation of PRS-Bridge is freely available on GitHub at <https://github.com/YuzhengDun1999/PRSBridge>.

## Acknowledgement

This work was supported by the following NIH grants: R01 HG010480 (Y.D., J.J., N.C.), R00 HG012223 (J.J.), and U01 CA249866 (N.C.). Individual-level genotype and phenotype data of the UK Biobank samples were obtained under application 17731.

## References

Tyler M Seibert, Chun Chieh Fan, Yunpeng Wang, Verena Zuber, Roshan Karunamuni, J Kellogg Parsons, Rosalind A Eeles, Douglas F Easton, ZSofia Kote-Jarai, Ali Amin Al Olama, et al. Polygenic hazard score to guide screening for aggressive prostate cancer: development and validation in large scale cohorts. *bmj*, 360, 2018.

Emil Uffelmann, Qin Qin Huang, Nchangwi Syntia Munung, Jantina De Vries, Yukinori Okada, Alicia R Martin, Hilary C Martin, Tuuli Lappalainen, and Danielle Posthuma. Genome-wide association studies. *Nature Reviews Methods Primers*, 1(1):59, 2021.

Nilanjan Chatterjee, Jianxin Shi, and Montserrat García-Closas. Developing and evaluating polygenic risk prediction models for stratified disease prevention. *Nature Reviews Genetics*, 17(7):392–406, 2016.

Pradeep Natarajan, Robin Young, Nathan O. Stitzel, Sandosh Padmanabhan, Usman Baber, Roxana Mehran, Samantha Sartori, Valentin Fuster, Dermot F. Reilly, Adam Butterworth, Daniel J. Rader, Ian Ford, Naveed Sattar, and Sekar Kathiresan. Polygenic risk score identifies subgroup with higher burden of atherosclerosis and greater relative benefit from statin therapy in the primary prevention setting. *Circulation*, 135(22):2091–2101, 2017. doi: 10.1161/CIRCULATIONAHA.116.024436. URL <https://www.ahajournals.org/doi/abs/10.1161/CIRCULATIONAHA.116.024436>.

Amit V Khera, Mark Chaffin, Krishna G Aragam, Mary E Haas, Carolina Roselli, Seung Hoan Choi, Pradeep Natarajan, Eric S Lander, Steven A Lubitz, Patrick T Ellinor, et al. Genome-wide polygenic scores for common diseases individuals with risk equivalent to monogenic mutations. *Nature genetics*, 50(9):1219–1224, 2018.

Ali Torkamani, Nathan E Wineinger, and Eric J Topol. The personal and clinical utility of polygenic risk scores. *Nature Reviews Genetics*, 19(9):581–590, 2018.

Samuel A Lambert, Gad Abraham, and Michael Inouye. Towards clinical utility of polygenic risk scores. *Human molecular genetics*, 28(R2):R133–R142, 2019.

Iftikhar J Kullo, Cathryn M Lewis, Michael Inouye, Alicia R Martin, Samuli Ripatti, and Nilanjan Chatterjee. Polygenic scores in biomedical research. *Nature Reviews Genetics*, pages 1–9, 2022.

Gustavo de los Campos, Daniel Gianola, and David B. Allison. Predicting genetic predisposition in humans: the promise of whole-genome markers. *Nature Reviews Genetics*, 11(12):880–886, 2010.

Bjarni J Vilhjálmsson, Jian Yang, Hilary K Finucane, Alexander Gusev, Sara Lindström, Stephan Ripke, Giulio Genovese, Po-Ru Loh, Gaurav Bhatia, Ron Do, et al. Modeling linkage disequilibrium increases accuracy of polygenic risk scores. *The american journal of human genetics*, 97(4):576–592, 2015.

Xiang Zhu and Matthew Stephens. Bayesian large-scale multiple regression with summary statistics from genome-wide association studies. *The annals of applied statistics*, 11(3):1561, 2017.

Luke R Lloyd-Jones, Jian Zeng, Julia Sidorenko, Loïc Yengo, Gerhard Moser, Kathryn E

- Kemper, Huanwei Wang, Zhili Zheng, Reedik Magi, Tõnu Esko, et al. Improved polygenic prediction by bayesian multiple regression on summary statistics. *Nature communications*, 10(1):1–11, 2019.
- Tian Ge, Chia-Yen Chen, Yang Ni, Yen-Chen Anne Feng, and Jordan W Smoller. Polygenic prediction via bayesian regression and continuous shrinkage priors. *Nature communications*, 10(1):1–10, 2019.
- Florian Privé, Julyan Arbel, and Bjarni J Vilhjálmsson. LDpred2: better, faster, stronger. *Bioinformatics*, 36(22-23):5424–5431, 12 2020. ISSN 1367-4803. doi: 10.1093/bioinformatics/btaa1029. URL <https://doi.org/10.1093/bioinformatics/btaa1029>.
- Yiming Hu, Qiongshi Lu, Ryan Powles, Xinwei Yao, Can Yang, Fang Fang, Xinran Xu, and Hongyu Zhao. Leveraging functional annotations in genetic risk prediction for human complex diseases. *PLoS computational biology*, 13(6):e1005589, 2017.
- Carla Márquez-Luna, Steven Gazal, Po-Ru Loh, Samuel S Kim, Nicholas Furlotte, Adam Auton, and Alkes L Price. Incorporating functional priors improves polygenic prediction accuracy in uk biobank and 23andme data sets. *Nature Communications*, 12(1):6052, 2021.
- Timothy Shin Heng Mak, Robert Milan Porsch, Shing Wan Choi, Xueya Zhou, and Pak Chung Sham. Polygenic scores via penalized regression on summary statistics. *Genetic epidemiology*, 41(6):469–480, 2017.
- Gao Wang, Abhishek Sarkar, Peter Carbonetto, and Matthew Stephens. A simple new approach to variable selection in regression, with application to genetic fine mapping.

*Journal of the Royal Statistical Society Series B: Statistical Methodology*, 82(5):1273–1300, 2020.

Jack Pattee and Wei Pan. Penalized regression and model selection methods for polygenic scores on summary statistics. *PLoS computational biology*, 16(10):e1008271, 2020.

Ting-Huei Chen, Nilanjan Chatterjee, Maria Teresa Landi, and Jianxin Shi. A penalized regression framework for building polygenic risk models based on summary statistics from genome-wide association studies and incorporating external information. *Journal of the American Statistical Association*, 116(533):133–143, 2021.

Yan Zhang, Guanghao Qi, Ju-Hyun Park, and Nilanjan Chatterjee. Estimation of complex effect-size distributions using summary-level statistics from genome-wide association studies across 32 complex traits. *Nature genetics*, 50(9):1318–1326, 2018.

Nicholas G Polson, James G Scott, and Jesse Windle. The bayesian bridge. *Journal of the Royal Statistical Society: Series B (Statistical Methodology)*, 76(4):713–733, 2014.

Carlos M Carvalho, Nicholas G Polson, and James G Scott. Handling sparsity via the horseshoe. In *Artificial intelligence and statistics*, pages 73–80. PMLR, 2009.

Akihiko Nishimura and Marc A. Suchard. Prior-preconditioned conjugate gradient method for accelerated gibbs sampling in “large n, large p” bayesian sparse regression. *Journal of the American Statistical Association*, 0(0):1–14, 2022. doi: 10.1080/01621459.2022.2057859. URL <https://doi.org/10.1080/01621459.2022.2057859>.

Nayanah Siva. 1000 genomes project. *Nature biotechnology*, 26(3):256–257, 2008.

Andrew Gelman and T. P. Speed. Characterizing a joint probability distribution by con-

- ditionals. *Journal of the Royal Statistical Society. Series B (Methodological)*, 55(1): 185–188, 1993. ISSN 00359246. URL <http://www.jstor.org/stable/2346074>.
- James P Hobert and George Casella. Functional compatibility, Markov chains, and Gibbs sampling with improper posteriors. *Journal of Computational and Graphical Statistics*, 7(1):42–60, 1998.
- Florian Privé, Hugues Aschard, Andrey Ziyatdinov, and Michael GB Blum. Efficient analysis of large-scale genome-wide data with two r packages: bigstatsr and bigsnpr. *Bioinformatics*, 34(16):2781–2787, 2018.
- Trevor Park and George Casella. The Bayesian Lasso. *Journal of the american statistical association*, 103(482):681–686, 2008.
- Haoyu Zhang, Jianan Zhan, Jin Jin, Jingning Zhang, Wenxuan Lu, Ruzhang Zhao, Thomas U Ahearn, Zhi Yu, Jared O’Connell, Yunxuan Jiang, et al. A new method for multiancestry polygenic prediction improves performance across diverse populations. *Nature Genetics*, pages 1–12, 2023.
- Gary L Gadbury, Qinfang Xiang, Lin Yang, Stephen Barnes, Grier P Page, and David B Allison. Evaluating statistical methods using plasmode data sets in the age of massive public databases: an illustration using false discovery rates. *PLoS genetics*, 4(6): e1000098, 2008.
- Zhan Su, Jonathan Marchini, and Peter Donnelly. Hapgen2: simulation of multiple disease snps. *Bioinformatics*, 27(16):2304–2305, 2011.
- Paul DP Pharoah, Antonis Antoniou, Martin Bobrow, Ron L Zimmern, Douglas F Easton,

- and Bruce AJ Ponder. Polygenic susceptibility to breast cancer and implications for prevention. *Nature genetics*, 31(1):33–36, 2002.
- Nilanjan Chatterjee, Bill Wheeler, Joshua Sampson, Patricia Hartge, Stephen J Chanock, and Ju-Hyun Park. Projecting the performance of risk prediction based on polygenic analyses of genome-wide association studies. *Nature genetics*, 45(4):400–405, 2013.
- Zikun Yang, Chen Wang, Linxi Liu, Atlas Khan, Annie Lee, Badri Vardarajan, Richard Mayeux, Krzysztof Kiryluk, and Iuliana Ionita-Laza. Carma is a new bayesian model for fine-mapping in genome-wide association meta-analyses. *Nature Genetics*, 55:1057–1065, 2023. doi: 10.1038/s41588-023-01392-0.
- Roger A. Horn and Charles R. Johnson. *Matrix Analysis*. Cambridge University Press, 2012.
- Luc Devroye. Nonuniform random variate generation. *Handbooks in operations research and management science*, 13:83–121, 2006.
- Tomaz Berisa and Joseph K. Pickrell. Approximately independent linkage disequilibrium blocks in human populations. *Bioinformatics*, 32(2):283–285, 09 2015. ISSN 1367-4803. doi: 10.1093/bioinformatics/btv546. URL <https://doi.org/10.1093/bioinformatics/btv546>.
- Florian Privé, Julyan Arbel, Hugues Aschard, and Bjarni J Vilhjálmsson. Identifying and correcting for misspecifications in gwas summary statistics and polygenic scores. *Human Genetics and Genomics Advances*, 3(4):100136, 2022.
- Christopher C Chang, Carson C Chow, Laurent CAM Tellier, Shashaank Vattikuti, Shaun M Purcell, and James J Lee. Second-generation PLINK: rising to the chal-



lenge of larger and richer datasets. *GigaScience*, 4(1):s13742–015–0047–8, 02 2015. ISSN 2047-217X. doi: 10.1186/s13742-015-0047-8. URL <https://doi.org/10.1186/s13742-015-0047-8>.

Kyriaki Michailidou, Sara Lindström, Joe Dennis, Jonathan Beesley, Shirley Hui, Siddhartha Kar, Audrey Lemaçon, Penny Soucy, Dylan Glubb, Asha Rostamianfar, et al. Association analysis identifies 65 new breast cancer risk loci. *Nature*, 551(7678):92–94, 2017.

A comprehensive 1000 genomes–based genome-wide association meta-analysis of coronary artery disease. *Nature genetics*, 47(10):1121–1130, 2015.

Naomi R Wray, Stephan Ripke, Manuel Mattheisen, Maciej Trzaskowski, Enda M Byrne, Abdel Abdellaoui, Mark J Adams, Esben Agerbo, Tracy M Air, Till MF Andlauer, et al. Genome-wide association analyses identify 44 risk variants and refine the genetic architecture of major depression. *Nature genetics*, 50(5):668–681, 2018.

Jimmy Z Liu, Suzanne Van Sommeren, Hailiang Huang, Siew C Ng, Rudi Alberts, Atsushi Takahashi, Stephan Ripke, James C Lee, Luke Jostins, Tejas Shah, et al. Association analyses identify 38 susceptibility loci for inflammatory bowel disease and highlight shared genetic risk across populations. *Nature genetics*, 47(9):979–986, 2015.

Yukinori Okada, Di Wu, Gosia Trynka, Towfique Raj, Chikashi Terao, Katsunori Ikari, Yuta Kochi, Koichiro Ohmura, Akari Suzuki, Shinji Yoshida, et al. Genetics of rheumatoid arthritis contributes to biology and drug discovery. *Nature*, 506(7488):376–381, 2014.

## Appendix

## A. Theorem 1: Proof and Real Data Demonstration

In this section, we prove the Theorem 1 and demonstrate, as we have done for Theorem 2 in Section 2.3, its consequence with real data.

*Proof of Theorem 1.* Let  $\mathbf{D}_{\text{ref}} = \mathbf{V}_{\text{ref}}\mathbf{\Delta}_{\text{ref}}\mathbf{V}_{\text{ref}}^T$  denote the eigenvalue decomposition of the LD correlation matrix estimated from external reference data. To establish the claimed behaviors of the nominal posterior, we first express the posterior mean in terms of the eigenvalues and eigenvectors of  $\mathbf{D}_{\text{ref}}$  as

$$\begin{aligned}\hat{\boldsymbol{\mu}} &= (N_{\text{train}}\mathbf{D}_{\text{ref}} + \sigma_0^{-2}\mathbf{I})^{-1}N_{\text{train}}\tilde{\boldsymbol{\beta}}_{\text{train}}^{(\text{sum})} \\ &= \mathbf{V}_{\text{ref}}\left(\mathbf{\Delta}_{\text{ref}} + \frac{1}{N_{\text{train}}}\sigma_0^{-2}\mathbf{I}\right)^{-1}\mathbf{V}_{\text{ref}}^T\tilde{\boldsymbol{\beta}}_{\text{train}}^{(\text{sum})} \\ &= \sum_{\ell=1}^P \frac{\langle \mathbf{v}_{\text{ref},\ell}, \tilde{\boldsymbol{\beta}}_{\text{train}}^{(\text{sum})} \rangle}{\delta_{\text{ref},\ell} + \frac{1}{N_{\text{train}}}\sigma_0^{-2}} \mathbf{v}_{\text{ref},\ell},\end{aligned}$$

where  $\delta_{\text{ref},\ell} \geq 0$  and  $\mathbf{v}_{\text{ref},\ell}$  denote the eigenvalues and eigenvectors of  $\mathbf{D}_{\text{ref}}$ . We can hence express the squared norm of  $\hat{\boldsymbol{\mu}}$  as

$$\|\hat{\boldsymbol{\mu}}\|^2 = \sum_{\ell=1}^P \frac{\langle \mathbf{v}_{\text{ref},\ell}, \tilde{\boldsymbol{\beta}}_{\text{train}}^{(\text{sum})} \rangle^2}{\left(\delta_{\text{ref},\ell} + \frac{1}{N_{\text{train}}}\sigma_0^{-2}\right)^2}. \quad (8)$$

We now use the Equation (8) to study the behavior of  $\|\hat{\boldsymbol{\mu}}\|$ . We first consider the mismatched case  $\text{null}(\mathbf{D}_{\text{ref}}) \not\subseteq \text{null}(\mathbf{D}_{\text{train}})$ . This means that there exists an eigenvector  $\mathbf{v}_{\text{ref},k}$  such that  $\mathbf{v}_{\text{ref},k} \in \text{null}(\mathbf{D}_{\text{ref}})$  and  $\mathbf{v}_{\text{ref},k} \notin \text{null}(\mathbf{D}_{\text{train}})$  with corresponding eigenvalue  $\delta_{\text{ref},k} = 0$ . By Assumption 1, we have  $\langle \mathbf{v}_{\text{ref},k}, \tilde{\boldsymbol{\beta}}_{\text{train}}^{(\text{sum})} \rangle \neq 0$  holds for almost every realization of summary statistics. For such summary statistics, the Equation (8) tells us that

$$\|\hat{\boldsymbol{\mu}}\| \geq N_{\text{train}}\sigma_0^2 |\langle \mathbf{v}_{\text{ref},k}, \tilde{\boldsymbol{\beta}}_{\text{train}}^{(\text{sum})} \rangle|,$$

where the right hand side tends to  $\infty$  as  $\sigma_0 \rightarrow \infty$ .

We now consider the other case  $\text{null}(\mathbf{D}_{\text{ref}}) \subseteq \text{null}(\mathbf{D}_{\text{train}})$ . In this case, since  $\tilde{\boldsymbol{\beta}}_{\text{train}}^{(\text{sum})} \in \text{col}(\mathbf{D}_{\text{train}}) = \text{null}(\mathbf{D}_{\text{train}})^\perp$ , we have  $\langle \mathbf{v}_{\text{ref},k}, \tilde{\boldsymbol{\beta}}_{\text{train}}^{(\text{sum})} \rangle = 0$  for every eigenvector  $\mathbf{v}_{\text{ref},k} \in$

$\text{null}(\mathbf{D}_{\text{ref}}) \subseteq \text{null}(\mathbf{D}_{\text{train}})$  associated with zero eigenvalue. Hence the Equation (8) becomes

$$\|\hat{\boldsymbol{\mu}}\|^2 = \sum_{\ell: \delta_{\text{ref},\ell} \neq 0} \frac{\langle \mathbf{v}_{\text{ref},\ell}, \tilde{\boldsymbol{\beta}}_{\text{train}}^{(\text{sum})} \rangle^2}{\left( \delta_{\text{ref},\ell} + \frac{1}{N_{\text{train}}} \sigma_0^{-2} \right)^2} \leq \sum_{\ell: \delta_{\text{ref},\ell} \neq 0} \frac{\langle \mathbf{v}_{\text{ref},\ell}, \tilde{\boldsymbol{\beta}}_{\text{train}}^{(\text{sum})} \rangle^2}{\delta_{\text{ref},\ell}^2} < \infty.$$

The norm  $\|\hat{\boldsymbol{\mu}}\|$  thus remains bounded even as  $\sigma_0 \rightarrow \infty$ .  $\square$

We now demonstrate the consequence of Theorem 1 in the matched and mismatched cases using real data. We use data from UK Biobank and consider BMI as an outcome and 200 consecutive SNPs from the first LD block of chromosome 22 as predictors. For the matched case, we obtain both summary-statistics and LD matrix from the same approximately 37K unrelated white individuals. For the unmatched case, we obtain the input data of the same size but from two distinct sets of individuals. Supplementary Figure 1 plots the posterior mean as a function of  $\sigma_0$  under these two scenarios, clearly demonstrating the two distinct behaviors of the posterior as predicted by the theorem.

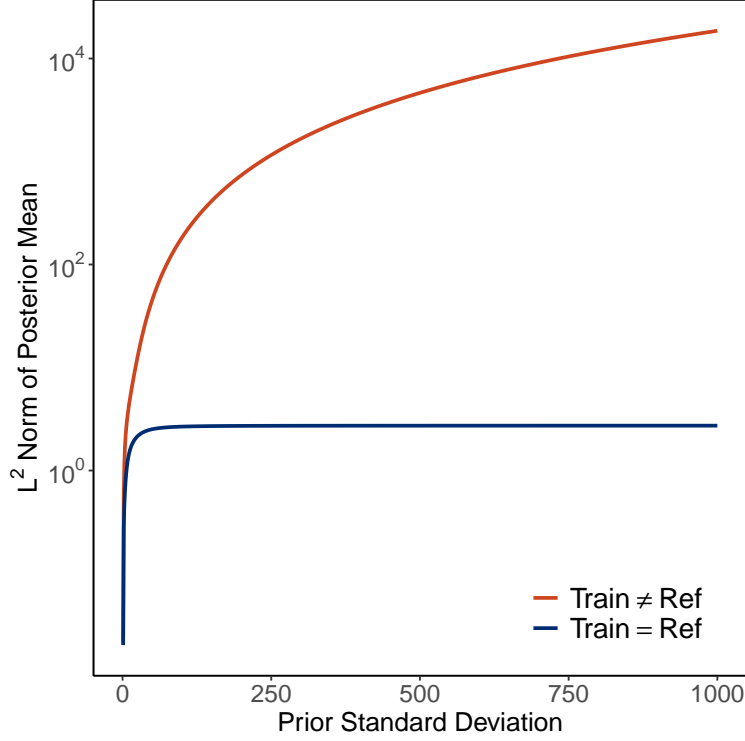
## B. Proof of Theorem 2

A heavy-tailed distribution can intuitively thought of as a distribution whose density has tails that decay slower than exponentials. More formally, it is defined as follows:

**Definition 1** (Heavy-tailed distribution). A distribution with density  $\pi(\cdot)$  and cumulative distribution  $F(\cdot)$  is said to be *heavy-tailed* if  $\int_{-\infty}^{\infty} \pi(x) \exp(tx) dx = \infty$  for any  $t > 0$  or, equivalently, if  $\lim_{x \rightarrow \infty} \exp(tx)(1 - F(x)) = \infty$ .

We first establish three lemmas to be use for our proof of Theorem 2:

**Lemma 1.** *Suppose  $\pi(\beta)$  admits a scale mixture representation  $\pi(\beta | \lambda^2) \sim \mathcal{N}(0, \lambda^2)$  with  $\lambda^2 \sim \pi(\lambda^2)$ . Then  $\pi(\beta)$  is heavy-tailed if and only if  $\pi(\lambda^2)$  is heavy-tailed.*



Supplementary Figure 1: The  $L^2$  norm of the posterior mean of  $\beta$  under different values of the prior standard deviation  $\sigma_0$  when the reference sample matches the training sample ( $\mathbf{D}_{\text{ref}} = \mathbf{D}_{\text{train}}$ , blue curve) and when the reference sample does not match the training sample ( $\mathbf{D}_{\text{ref}} \neq \mathbf{D}_{\text{train}}$ , red curve).

*Proof.* By Tonelli's theorem, we have for any  $t > 0$

$$\begin{aligned}
& \int_{-\infty}^{\infty} \pi(\beta) \exp(t\beta) d\beta \\
&= \int_{-\infty}^{\infty} \int_0^{\infty} \pi(\beta | \lambda^2) \pi(\lambda^2) \exp(t\beta) d\lambda^2 d\beta \\
&= \int_0^{\infty} \int_{-\infty}^{\infty} \pi(\beta | \lambda^2) \pi(\lambda^2) \exp(t\beta) d\beta d\lambda^2 \\
&= \int_0^{\infty} \int_{-\infty}^{\infty} (2\pi\lambda^2)^{-1/2} \pi(\lambda^2) \exp\left(-\frac{\beta^2 - 2\lambda^2 t\beta}{2\lambda^2}\right) d\beta d\lambda^2 \\
&= \int_0^{\infty} \pi(\lambda^2) \exp\left(\frac{\lambda^2 t^2}{2}\right) d\lambda^2
\end{aligned} \tag{9}$$

Hence  $\int_{-\infty}^{\infty} \pi(\beta) \exp(t\beta) d\beta = \infty$  if and only if  $\int_0^{\infty} \pi(\lambda^2) \exp\left(\frac{\lambda^2 t^2}{2}\right) d\lambda^2 = \infty$ .  $\square$

**Lemma 2.** *If a density  $\pi(x)$  on  $x \geq 0$  is heavy-tailed, then  $\pi'(x) \propto (1 + \delta x)^{-1/2} \pi(x)$  is also heavy-tailed for any  $\delta > 0$ .*

*Proof.* Denote the reciprocal of the normalizing constant by  $C = (\int \pi'(x) dx)^{-1}$  and let  $t > 0$ . Observe that

$$\begin{aligned}
& \int_0^\infty \pi'(x) \exp(tx) dx \\
&= C \int_0^\infty (\delta x + 1)^{-1/2} \pi(x) \exp(tx) dx \\
&= C \int_0^\infty \pi(x) \exp\left(\frac{tx}{2}\right) \frac{\exp\left(\frac{tx}{2}\right)}{\sqrt{\delta x + 1}} dx \\
&\geq C \int_L^\infty \pi(x) \exp\left(\frac{tx}{2}\right) dx.
\end{aligned} \tag{10}$$

The last inequality comes from the fact that there exists  $L < \infty$  such that  $\exp(tx/2) > (\delta x + 1)^{1/2}$  for all  $x > L$ . Since  $\pi(x)$  is heavy-tailed and  $\int_0^\infty \pi(x) \exp\left(\frac{tx}{2}\right) dx = \infty$ , we must also have  $\int_L^\infty \pi(x) \exp\left(\frac{tx}{2}\right) dx = \infty$ .  $\square$

**Lemma 3.** *Suppose that  $X_1, X_2, \dots, X_n$  are i.i.d. random variables with cumulative distribution  $F_X(\cdot)$ . Let  $Y = \min(X_1, X_2, \dots, X_n)$  and denote its cumulative distribution by  $F_Y(\cdot)$ . If  $F_X(\cdot)$  is heavy-tailed, then so is  $F_Y(\cdot)$ .*

*Proof.* Since the distribution of  $X_1, X_2, \dots, X_n$  is heavy-tailed, by definition we have

$$\lim_{x \rightarrow \infty} \exp(tx)(1 - F_X(x)) = \infty \text{ for any } t > 0.$$

It follows that, for any  $n > 0$ ,

$$\lim_{x \rightarrow \infty} \exp(ntx)(1 - F(x))^n = \left( \lim_{x \rightarrow \infty} \exp(tx)(1 - F(x)) \right)^n = \infty \text{ for any } t > 0.$$

Since the cumulative density of  $Y = \min(X_1, \dots, X_n)$  is given by  $F_Y(y) = 1 - [1 - F_X(y)]^n$ , we have for any  $s > 0$

$$\lim_{y \rightarrow \infty} \exp(sy)(1 - F_Y(y)) = \lim_{y \rightarrow \infty} \exp(nty)[1 - F_X(y)]^n = \infty \text{ for } t = s/n > 0.$$

As this holds for any  $s > 0$ , the distribution of  $Y$  is heavy-tailed.  $\square$

We proceed to the proof of Theorem 2:

*Proof of Theorem 2.* Consider a prior  $\beta_j | \tau, \lambda_j \sim \mathcal{N}(0, \tau^2 \lambda_j^2)$  with  $\lambda_j^2 \sim \pi(\lambda_j^2)$ . Denote  $\mathbf{\Lambda} = \text{diag}(\lambda_1, \dots, \lambda_P)$  and  $\mathbf{\Phi} = N_{\text{train}} \mathbf{D}_{\text{ref}} + \tau^{-2} \mathbf{\Lambda}^{-2}$ . Setting  $\hat{\boldsymbol{\beta}} = \mathbf{0}$  in Equation (6), we obtain the following relation for the joint nominal posterior:

$$\begin{aligned}
& \pi\left(\boldsymbol{\beta}, \lambda_1^2, \dots, \lambda_P^2 \mid \tilde{\boldsymbol{\beta}}_{\text{train}}^{(\text{sum})}, \mathbf{D}_{\text{ref}}, \tau\right) \\
& \propto \frac{\exp\left(-\frac{(\boldsymbol{\beta} - N_{\text{train}} \mathbf{\Phi}^{-1} \tilde{\boldsymbol{\beta}}_{\text{train}}^{(\text{sum})})^T \mathbf{\Phi} (\boldsymbol{\beta} - N_{\text{train}} \mathbf{\Phi}^{-1} \tilde{\boldsymbol{\beta}}_{\text{train}}^{(\text{sum})})}{2}\right) \prod_{j=1}^P \lambda_j^{-1} \pi(\lambda_j^2)}{\exp\left(-\frac{(N_{\text{train}} \mathbf{\Phi}^{-1} \tilde{\boldsymbol{\beta}}_{\text{train}}^{(\text{sum})})^T \mathbf{\Phi} (N_{\text{train}} \mathbf{\Phi}^{-1} \tilde{\boldsymbol{\beta}}_{\text{train}}^{(\text{sum})})}{2}\right)} \\
& = \exp\left(-\frac{\boldsymbol{\beta}^T \mathbf{\Phi} \boldsymbol{\beta} - 2 \boldsymbol{\beta}^T N_{\text{train}} \tilde{\boldsymbol{\beta}}_{\text{train}}^{(\text{sum})}}{2}\right) \prod_{j=1}^P \lambda_j^{-1} \pi(\lambda_j^2) \\
& = (2\pi)^{-P/2} \varphi\left(\boldsymbol{\beta} \mid \mathbf{\Phi}^{-1} N_{\text{train}} \tilde{\boldsymbol{\beta}}_{\text{train}}^{(\text{sum})}, \mathbf{\Phi}^{-1}\right) \\
& \quad \det(\mathbf{\Phi})^{-1/2} \exp\left(-\frac{N_{\text{train}}^2 \left(\tilde{\boldsymbol{\beta}}_{\text{train}}^{(\text{sum})}\right)^T \mathbf{\Phi}^{-1} \tilde{\boldsymbol{\beta}}_{\text{train}}^{(\text{sum})}}{2}\right) \prod_{j=1}^P \lambda_j^{-1} \pi(\lambda_j^2),
\end{aligned} \tag{11}$$

where  $\varphi(\boldsymbol{\beta} \mid \boldsymbol{\mu}, \boldsymbol{\Sigma})$  denotes the normal probability density function with mean  $\boldsymbol{\mu}$  and variance  $\boldsymbol{\Sigma}$  evaluated at  $\boldsymbol{\beta}$ . In addition, we have

$$\begin{aligned}
& \tau^{-1} \det(\mathbf{\Phi})^{-1/2} \prod_{j=1}^P \lambda_j^{-1} \\
& = \det(N_{\text{train}} \tau^2 \mathbf{\Lambda} \mathbf{D}_{\text{ref}} \mathbf{\Lambda} + \mathbf{I})^{-1/2} \\
& = \det(N_{\text{train}} \tau^2 \mathbf{\Lambda} \mathbf{V}_{\text{ref}} \boldsymbol{\Delta}_{\text{ref}} \mathbf{V}_{\text{ref}}^T \mathbf{\Lambda} + \mathbf{I})^{-1/2} \\
& \geq \det(N_{\text{train}} \delta_{\text{ref, max}} \tau^2 \mathbf{\Lambda}^2 + \mathbf{I})^{-1/2} \\
& = \prod_{j=1}^P (N_{\text{train}} \tau^2 \lambda_j^2 \delta_{\text{ref, max}} + 1)^{-1/2},
\end{aligned} \tag{12}$$

where  $\delta_{\text{ref, max}}$  is the largest eigenvalue of  $\mathbf{D}_{\text{ref}}$ ; the inequality of the determinants follow from the fact  $(N_{\text{train}} \tau^2 \mathbf{\Lambda} \mathbf{V}_{\text{ref}} \boldsymbol{\Delta}_{\text{ref}} \mathbf{V}_{\text{ref}}^T \mathbf{\Lambda} + \mathbf{I}) \succ (N_{\text{train}} \delta_{\text{ref, max}} \tau^2 \mathbf{\Lambda}^2 + \mathbf{I})$  and Weyl's inequality [Horn and Johnson, 2012].

Denote by  $\pi'(\lambda_j^2)$  the density proportional to  $(N_{\text{train}}\tau^2\lambda_j^2\delta_{\text{ref,max}} + 1)^{-1/2}\pi(\lambda_j^2)$ . Also denote  $\lambda_{\min}^2 = \min(\lambda_1^2, \dots, \lambda_P^2)$ . Now observe that

$$\begin{aligned}
& \int \pi(\boldsymbol{\beta}, \lambda_1^2, \dots, \lambda_P^2 \mid \tilde{\boldsymbol{\beta}}_{\text{train}}^{(\text{sum})}, \mathbf{D}_{\text{ref}}, \tau) d\boldsymbol{\beta} d\lambda_1^2 \dots d\lambda_P^2 \\
&= C_1 \int \det(\boldsymbol{\Phi})^{-1/2} \exp\left(\frac{N_{\text{train}}^2 (\tilde{\boldsymbol{\beta}}_{\text{train}}^{(\text{sum})})^T \boldsymbol{\Phi}^{-1} \tilde{\boldsymbol{\beta}}_{\text{train}}^{(\text{sum})}}{2}\right) \prod_{j=1}^P \lambda_j^{-1} \pi(\lambda_j^2) d\lambda_1^2 \dots d\lambda_P^2 \\
&\geq C_1 \int \exp\left(\frac{N_{\text{train}}^2 (\tilde{\boldsymbol{\beta}}_{\text{train}}^{(\text{sum})})^T \boldsymbol{\Phi}^{-1} \tilde{\boldsymbol{\beta}}_{\text{train}}^{(\text{sum})}}{2}\right) \prod_{j=1}^P (N_{\text{train}}\tau^2\lambda_j^2\delta_{\text{ref,max}} + 1)^{-1/2} \pi(\lambda_j^2) d\lambda_1^2 \dots d\lambda_P^2 \\
&= C_2 \int \exp\left(\frac{N_{\text{train}}^2 (\tilde{\boldsymbol{\beta}}_{\text{train}}^{(\text{sum})})^T \boldsymbol{\Phi}^{-1} \tilde{\boldsymbol{\beta}}_{\text{train}}^{(\text{sum})}}{2}\right) \prod_{j=1}^P \pi'(\lambda_j^2) d\lambda_1^2 \dots d\lambda_P^2 \\
&\geq C_3 \int \exp\left(\frac{N_{\text{train}} (\tilde{\boldsymbol{\beta}}_{\text{train}}^{(\text{sum})})^T \mathbf{V}_{\text{ref}} (\boldsymbol{\Delta}_{\text{ref}} + N_{\text{train}}^{-1} \tau^{-2} \lambda_{\min}^{-2} \mathbf{I})^{-1} \mathbf{V}_{\text{ref}}^T \tilde{\boldsymbol{\beta}}_{\text{train}}^{(\text{sum})}}{2}\right) \\
&\quad \pi'(\lambda_{\min}^2) \pi'(\lambda_1^2, \dots, \lambda_P^2 \mid \lambda_{\min}^2) d\lambda_1^2 \dots d\lambda_P^2 \\
&\geq C_4 \int \exp\left(\frac{N_{\text{train}} \langle \mathbf{v}_{\text{ref},k}, \tilde{\boldsymbol{\beta}}_{\text{train}}^{(\text{sum})} \rangle^2}{2(\delta_{\text{ref},k} + N_{\text{train}}^{-1} \tau^{-2} \lambda_{\min}^{-2})}\right) \pi'(\lambda_{\min}^2) d\lambda_{\min}^2,
\end{aligned} \tag{13}$$

where the first inequality follows from Equation (12), the second inequality follows from the fact  $\boldsymbol{\Phi} \prec \mathbf{V}_{\text{ref}}(N_{\text{train}}\boldsymbol{\Delta}_{\text{ref}} + \tau^{-2}\lambda_{\min}^{-2}\mathbf{I})\mathbf{V}_{\text{ref}}^T$  and holds for any  $k$ , and  $C_1, C_2, C_3, C_4$  are positive constants. The same logic as in the proof of Theorem 1 tells us when  $\text{null}(\mathbf{D}_{\text{ref}}) \not\subseteq \text{null}(\mathbf{D}_{\text{train}})$ , there exists an eigenvalue/vector pair  $(\delta_{\text{ref},k}, \mathbf{v}_{\text{ref},k})$ , such that  $\delta_{\text{ref},k} = 0$  and  $\langle \mathbf{v}_{\text{ref},k}, \tilde{\boldsymbol{\beta}}_{\text{train}}^{(\text{sum})} \rangle \neq 0$  for almost every realization of summary statistics. Now, by Lemma 1, 2, and 3, we know that  $\pi'(\lambda_{\min}^2)$  is heavy-tailed, and hence

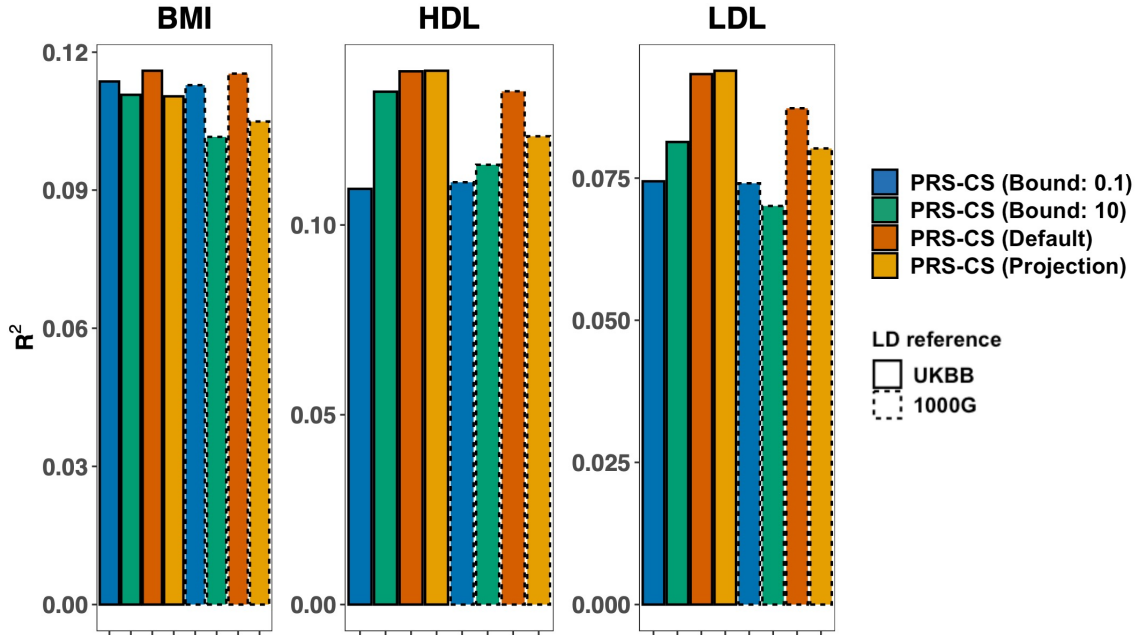
$$\int \exp\left(\frac{N_{\text{train}}^2 \tau^2 \langle \mathbf{v}_{\text{ref},k}, \tilde{\boldsymbol{\beta}}_{\text{train}}^{(\text{sum})} \rangle^2 \lambda_{\min}^2}{2}\right) \pi'(\lambda_{\min}^2) d\lambda_{\min}^2 = \infty. \tag{14}$$

Combining Equation (13) and (14), we conclude that the joint nominal posterior is improper.  $\square$

### C. PRS-CS Using Projected Summary Statistics

Here we compare the performance of PRS-CS using projected summary statistics against its original implementation based on the ad-hoc constraint of the form  $\tau^2 \lambda_j^2 \leq \sigma_{\text{bd}}^2$  on the prior variance of coefficients. For the projection-based version, we employ the same low-rank approximation of the LD matrix as used in PRS-Bridge. We treat the percentage of eigenvalue removed as tuning parameter, with values set at 20%, 40%, 60%, and 80%. As shown in Supplementary Figure 2, the constraint-based version is sensitive to the choice of  $\sigma_{\text{bd}}^2$ . The projection-based version achieves competitive performance, especially when the LD reference data source is sufficiently large as in UK Biobank. When the reference data source is small as in 1000G, the constraint-based version with tuned  $\sigma_{\text{bd}}$  appears to become the more attractive alternative. This is likely because, when its sample size is small, the population LD structure cannot be well estimated from the reference. Correspondingly, the projection ends up removing, along with the noise, useful information the summary statistics have about the target population.





Supplementary Figure 2: Out-of-sample prediction  $R^2$  of PRS-CS on the three continuous traits: BMI, high-density lipoprotein cholesterol (HDL), low-density lipoprotein cholesterol (LDL). We implement each method with two alternative LD reference data sources, 1000G and UK Biobank. “Bound” indicates the use of the bound on the prior variance of coefficients, which varies from 0.1, 1 (Default), to 10. “Projection” indicates the use of the projection approach.

## D. Details of Conjugate Gradient-accelerated Gibbs Sampler for PRS-Bridge

The Bridge prior can be expressed as a scale mixture of normal distributions as [Polson et al., 2014]:

$$\beta | \Lambda, \tau \sim \mathcal{N}(0, \tau^2 \Lambda^2), \quad \Lambda = \text{diag}(\lambda_j), \quad \pi(\lambda_j) \propto \lambda_j^{-2} \pi_{st}(\lambda_j^{-2}/2),$$

where  $\tau$  is the global scale parameter,  $\lambda_j$  the local scale parameter, and  $\pi_{st}$  is an alpha-stable distribution with an index of stability  $\alpha/2$ . The Gibbs sampler’s steps are as follows:

1. We first update  $\tau$  by sampling from  $\nu = \tau^{-\alpha}$  after marginalizing out  $\lambda_j$ 's. Assuming a Gamma prior  $\pi(\nu) \propto \nu^{k-1} e^{-\nu\theta}$  and after integrating out  $\lambda_j$ 's, the posterior conditional of  $\nu$  is given by

$$\nu | \boldsymbol{\beta} \propto \nu^{k+p/\alpha-1} \exp\left(-\nu\left(\theta + \sum_{j=1}^p |\beta_j|^\alpha\right)\right).$$

2. We next update  $\lambda_j$ 's. While the full conditional does not have a closed form formula, we can sample from it by using the double-rejection algorithm of Devroye [2006] as implemented in the Python package “bayesbridge” in Nishimura and Suchard [2022].
3. Finally, we update  $\boldsymbol{\beta}$  from its full conditional given by, for  $\boldsymbol{\Phi} = N\mathbf{D} + \tau^{-2}\boldsymbol{\Lambda}^{-2}$ ,

$$\boldsymbol{\beta} | \boldsymbol{\beta}_{\text{sum}}, \boldsymbol{\Lambda}, \tau \sim \mathcal{N}(\boldsymbol{\Phi}^{-1}N\boldsymbol{\beta}_{\text{sum}}, \boldsymbol{\Phi}^{-1}). \quad (15)$$

The highest computational cost arises from generating the multivariate normal distribution in (15). By partitioning the whole genome into independent LD blocks, we can update  $\boldsymbol{\beta}$  independently within LD block. To further speed up the computation, we use the conjugate gradient sampler of Nishimura and Suchard [2022] instead of the standard approach based on Cholesky decomposition of precision matrix. Specifically, we use a two-step procedure to sample from (15):

- 1) Generate a Gaussian vector  $\mathbf{b}$  from  $\mathcal{N}(N\boldsymbol{\beta}_{\text{sum}}, \boldsymbol{\Phi})$  by first generating two independent Gaussian vectors,  $\boldsymbol{\eta}$  from  $\mathcal{N}(0, \mathbf{I}_n)$ , and  $\boldsymbol{\delta}$  from  $\mathcal{N}(0, \mathbf{I}_p)$ , and then setting

$$\mathbf{b} = N\boldsymbol{\beta}_{\text{sum}} + N^{1/2}\mathbf{D}^{1/2}\boldsymbol{\eta} + \tau^{-1}\boldsymbol{\Lambda}^{-1}\boldsymbol{\delta}.$$

- 2) Solve the following linear system for  $\boldsymbol{\beta}$ :

$$\boldsymbol{\Phi}\boldsymbol{\beta} = \mathbf{b} \quad \text{where } \boldsymbol{\Phi} = N\mathbf{D} + \tau^{-2}\boldsymbol{\Lambda}^{-2}. \quad (16)$$

For step (2), we use the conjugate gradient method, which is an iterative method to solve the linear system whose computational cost is dominated by matrix-vector multiplication  $\Phi\beta$ . To speed up the convergence of the CG method, we combine it with the prior-preconditioning strategy developed by Nishimura and Suchard [2022].

## E. Details of Methods’ Implementations

The large number of genetic variants across the genome makes for an exceptionally high-dimensional problem. Within European populations only, there are over eight million bi-allelic SNPs with minor allele frequency above 1%. To keep the computation manageable, PRS methods typically use a pre-selected subset of SNPs, the HapMap 3 SNP list providing the most commonly used one. This list contains approximately 1.2 million SNPs that provide good coverage of the genome for European populations. Following this standard practice, we include in our analysis only the HapMap 3 bi-allelic SNPs to strike a balance between statistical power and computational feasibility.

For the implementation of LDpred2, we use the LDpred2-grid algorithm implemented in the R package “bigsnpr” (version 1.10.8) [Privé et al., 2018]. It conducts a grid search to estimate 1) the causal SNP proportion with candidate values being a sequence of 21 numbers evenly spaced on a logarithmic scale between  $10^{-5}$  and 1, and 2) the heritability parameter with the candidate values being the estimates from the LD score regression multiplied by 0.7, 1, or 1.4.

For PRS-CS, we treated global shrinkage parameter  $\tau$  as a tuning parameter and searched among its default candidate values suggested by the authors of PRS-CS,  $\{10^{-6}, 10^{-4}, 10^{-2}, 1\}$ . For our proposed PRS-Bridge, we treat the percentage of eigenvalues removed in the low-rank LD matrix approximation step as a tuning parameter with candidate values 0%, 20%,

40%, 60%, and 80%. The eigenvalues of magnitude less than 0.01 are always removed to prevent numerical instability. We also treat the exponent  $\alpha$  as a tuning parameter with candidate values 0.125, 0.25, and 0.5. All the tuning parameters are selected based on the methods’ performance on the tuning datasets.

For PRS-Bridge, we use a scientifically-informed prior on the global scale  $\tau$  by taking advantage of the closed-form conditional variance formula  $\text{var}(\beta_j | \tau) = \frac{\Gamma(3/\alpha)}{\Gamma(1/\alpha)}\tau^2$ . Having standardized the outcome and predictors to have unit variance, we can interpret the prior conditional variance of  $\beta_j$  as per-SNP heritability; i.e. how much each SNP on average explains the variability in the trait. We can leverage well-established methods such as the LD-score regression to estimate the per-SNP heritability and then use this estimate to construct an informative prior on  $\tau$ .

## F. Details of LD Approximation Strategy

To evaluate the impact of the choice of LD reference data on PRS methods’ performance, we consider two alternative data sources for LD reference: (1) the 1000G reference samples with 489 unrelated individuals of European ancestry, (2) the UK Biobank reference samples with 337,484 unrelated individuals of European ancestry.

We additionally evaluate the impact of the choice of LD structures on the model performance. We provide two options to construct LD matrix in PRS-Bridge. The first “small-block” option partitions the LD matrix into 1,703 independent blocks generated by the method of Berisa and Pickrell [2015], which has previously been successfully implemented in PRS-CS. Within chromosome 1, for example, we end up with 133 blocks with each consisting on average of 689 SNPs from the HapMap 3 SNP set. The second “large-block” option partition the LD matrix using the function `snp_ldsplit` in the R package

“bigsnpr,” which generates the same block LD matrix as in Privé et al. [2022]. Within chromosome 1, for example, this yields 36 blocks with each consisting on average of 2,500 SNPs.

For LDpred2, we consider both of the two LD structures described in the LDpred2 tutorial. The “large-block” version uses the same large-block LD structure as described above and used by PRS-Bridge. We use the block LD matrix estimate as provided by the LDpred2 software, which is essentially identical to the one used by PRS-Bridge except potentially for minor differences in the quality control procedure (Appendix G). The “banded” version uses a banded LD structure with a default LD radius of 3cM. The software does not provide a banded LD matrix estimate, so we estimate it using a random subset of 5,000 individuals from the UK Biobank reference samples. The sub-sampling is done to ease the computational burden of estimating the banded approximation; we experimented with the sample size of 500, 1,000, 2,000, and 5,000 and observed little improvement in the method’s predictive performance once the sample size reached 2,000.

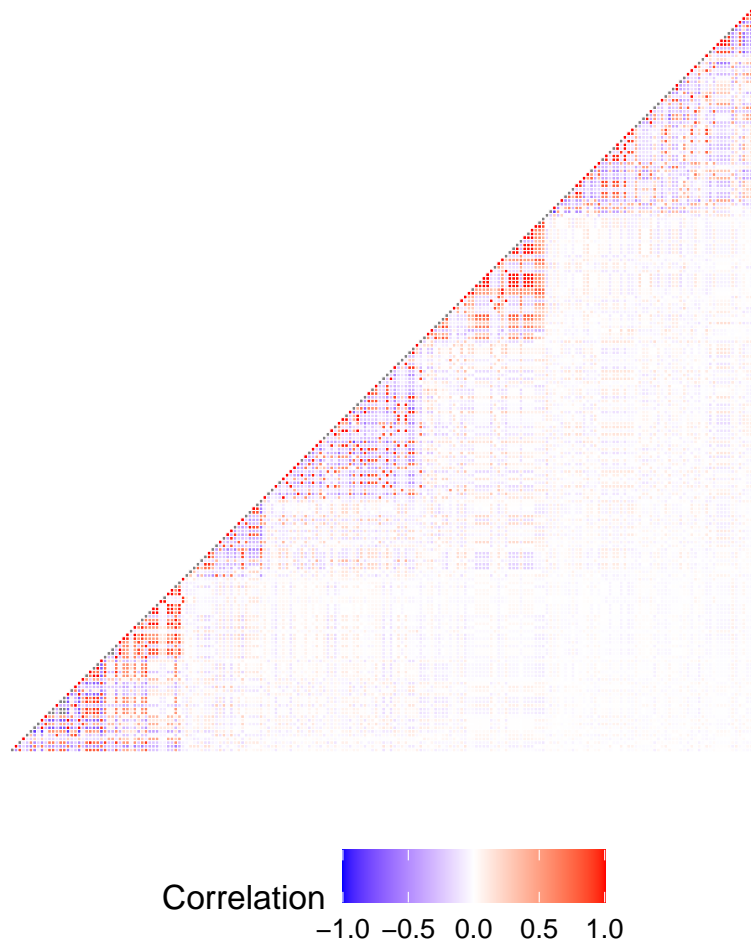
For PRS-CS, we consider the small-block LD structure provided as default in their software.

## G. Quality Control for UK Biobank and Summary Statistics Data

For the UK Biobank data used in Section 4.2 and 4.3, we apply the following quality control procedures. We restrict our analysis to unrelated genotyped European participants from the UK Biobank. We remove SNPs with minor allele frequency (MAF) below 0.01, missing rate over 0.05, and deviation from Hardy-Weinberg equilibrium with  $P < 10^{-7}$ .

For the GWAS summary statistics data used in Section 4.3, we remove SNPs (1) with low sample sizes ( $N_j < 0.9 \times \max(N_j)$ ) (2) with outlier marginal effect size  $\left(\frac{\hat{\beta}_j}{\sqrt{N\text{SE}(\hat{\beta}_j)}}\right)^2 > 80$ ;

## An Example Heatmap of LD Matrix



Supplementary Figure 3: Heatmap of the LD correlation matrix for the 200 SNPs, selected for the purpose of illustration, within an LD block (GRCh37 position: 17284065–17661178) on chromosome 22. The matrix is estimated from unrelated European individuals from UK Biobank with complete genotype information.

(3) in the long-range LD region of the position 25-35 Megabase in chromosome 6; (4) with MAF below 0.01.

We use PLINK [Chang et al., 2015] software for the above quality control.

## H. Runtime for prediction in UK Biobank

Here we compare the computational efficiency of PRS-Bridge with LDpred2 and PRS-CS. We train PRS models using BMI chromosome 22 summary statistics from UK Biobank study for the three methods under various LD matrix assumptions. We benchmark the methods' computational speed on Intel(R) Xeon(R) Silver 4310 CPU at 2.10 GHz in the single threaded setting. The results, as summarized in Supplementary Table 1, show that PRS-Bridge (Small-block) is on average 3.7 times faster than PRS-CS (Small-block) for each tuning setting. This allows PRS-Bridge (Small-block) to explore more tuning settings in the comparable amount of time, with an opportunity to further speed up the process by training each tuning setting in an embarrassingly parallel manner. PRS-Bridge (Large-block) takes roughly twice the computational time of PRS-Bridge (Small-block) since updating each block of the coefficients requires sampling from multivariate normal distributions of higher dimensions. LDpred2 (Banded) and LDpred2 (Large-block) are faster than PRS-Bridge and PRS-CS; this is likely due to the multiple approximations they make in their posterior computation to enforce conditional independence among the coefficients and thus avoid having to sample from multivariate normal distributions.

Supplementary Table 1: Computational efficiency comparison of the three Bayesian PRS methods

Method	Total Time (s)	Total Tuning Settings	Average Time Per Tuning Setting (s)
PRS-Bridge (Small-block)	1294.36	15	86.29
PRS-Bridge (Large-block)	2592.93	15	172.86
PRS-CS (Small-block)	1315.92	4	328.98
LDpred2 (Banded)	188.48	63	2.99
LDpred2 (Large-block)	24.321	63	0.39



Supplementary Table 2: Information on five common complex diseases

Disease	GWAS reference	GWAS sample size (case/control)	Tuning sample size (case/control)	Validation sample size (case/control)
Breast cancer	Michailidou et al. [2017]	228951 (122977/105974)	4170 (2085/2085)	4170 (2085/2085)
Coronary artery disease	car [2015]	184305 (60801/123504)	16336 (6903/10000)	16677 (7151/10000)
Depression	Wray et al. [2018]	124430 (45645/97674)	9510 (3119/10000)	9844 (3264/10000)
Inflammatory bowel disease	Liu et al. [2015]	34652 (12882/21770)	5056 (1447/10000)	5275 (1519/10000)
Rheumatoid arthritis	Okada et al. [2014]	58284 (14361/43923)	6846 (2065/10000)	7205 (2197/10000)